Electrochemical-mechanical modeling of solid polymer electrolytes
Impact of mechanical stresses on Li-ion battery performance

Grazioli, Davide; Verners, Osvalds; Zadin, Vahur; Brandell, Daniel; Simone, Angelo

DOI
10.1016/j.electacta.2018.07.234

Publication date
2019

Document Version
Final published version

Published in
Electrochimica Acta

Electrochimica Acta 296 (2019) 1122–1141

Contents lists available at ScienceDirect

Electrochimica Acta

journal homepage: www.elsevier.com/locate/electacta

Electrochemical-mechanical modeling of solid polymer electrolytes: Impact of mechanical stresses on Li-ion battery performance

Davide Grazioli [a, *], Osvalds Verners [a], Vahur Zadin [b], Daniel Brandell [c], Angelo Simone [d, a]

[a] Faculty of Civil Engineering and Geosciences, Delft University of Technology, Stevinweg 1, 2628 CN Delft, the Netherlands
[b] IMS Lab, Institute of Technology, University of Tartu, Nooruse 1, 50411 Tartu, Estonia
[c] Department of Chemistry, Ångström Laboratory, Box 538, Uppsala University, 751 21 Uppsala, Sweden
[d] Department of Industrial Engineering, University of Padova, Via Venezia 1, 35131 Padua, Italy

ARTICLE INFO

Article history:
Received 24 April 2018
Received in revised form
30 June 2018
Accepted 31 July 2018
Available online 4 August 2018

Keywords:
Solid polymer electrolytes
Electrochemical-mechanical coupling
Partial molar volume
Mechanical properties
Battery performance

ABSTRACT

We analyze the effects of mechanical stresses arising in a solid polymer electrolyte (SPE) on the electrochemical performance of the electrolyte component of a lithium ion battery. The SPE is modeled with a coupled ionic conduction-deformation model that allows to investigate the effect of mechanical stresses induced by the redistribution of ions. The analytical solution is determined for a uniform planar cell operating under galvanostatic conditions with and without externally induced deformations. The roles of the polymer stiffness, internally-induced stresses, and thickness of the SPE layer are investigated. The results show that the predictions of the coupled model can strongly deviate from those obtained with an electrochemical model—up to +38% in terms of electrostatic potential difference across the electrolyte layer—depending on the combination of material properties and geometrical features. The predicted stress level in the SPE is considerable as it exceeds the threshold experimentally detected for irreversible deformation or fracture to occur in cells not subjected to external loading. We show that stresses induced by external solicitations can reduce the concentration gradient of ions across the electrolyte thickness and prevent salt depletion at the electrode-electrolyte interface.

1. Introduction

Solid polymer electrolytes present advantages with respect to their liquid counterpart in terms of safety [1], reduced risk of leakage, possibility of being cast in complex architectures [2], and multifunctionality [3], thus making them appealing for a wide range of applications including medical implants and structural batteries. The existence of a trade-off between electrochemical performance, usually evaluated in terms of ionic conductivity, and their mechanical stiffness is well established [4]. A quantification of the local stress and its impact on the ionic transport mechanism is however difficult to establish experimentally; a similar consideration holds for the evaluation of the local deformation (shrinkage/swelling) induced by ions redistribution. In particular, the conditions experienced by the SPE in a real battery may strongly differ from those replicated in an experiment [5]. Here we evaluate the impact of the mechanical properties of the SPE on its electrochemical response when it is considered as part of a battery with the aid of a coupled electrochemical-mechanical model.

The SPE undergoes deformations during cycling operations, either caused by the redistribution of ions or by the expansion/contraction of the active material [5]. The competition between stiffness and ionic conductivity in SPEs is well established from a material level perspective: modifications of the microstructure to enhance one of these features generally lead to a significant reduction of the other [4] as schematically shown in Fig. 1. Additionally, tests performed under unstretched and stretched conditions yield different ionic conductivity measurements on polymer electrolyte films [6–9], suggesting that the ionic conduction mechanism is altered by stresses and deformations. To the best of the authors' knowledge, however, there are no studies reporting the relation between stresses arising in the SPE and the electrical response at the system level, i.e., when the electrolyte is considered as a battery component. Such an investigation can be undertaken either by analytical or numerical modeling approaches, both strongly encouraged by Hallinan and Balsara [3] and Asp and

* Corresponding author.
E-mail addresses: d.grazioli@tudelft.nl (D. Grazioli), o.verners@tudelft.nl (O. Verners), vahur.zadin@ut.ee (V. Zadin), daniel.brandell@kemi.uu.se (D. Brandell), angelo.simone@unipd.it, a.simone@tudelft.nl (A. Simone).

https://doi.org/10.1016/j.electacta.2018.07.234

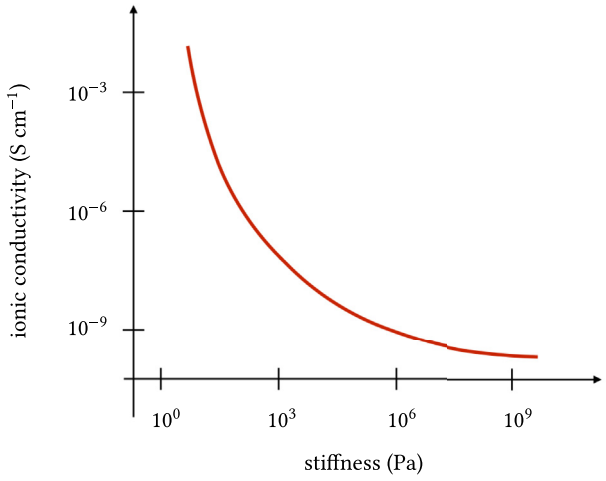

Fig. 1. Schematic of material level trend of lithium ion conductivity versus stiffness for SPE, redrawn according to Refs. [4,10].

Greenhalgh [4] in their recent review papers. The former is pursued in the current study, focused on uniform planar cells, while the latter is pursued in a companion paper [11], in which microbatteries with a trench geometry are considered.

While the literature on models that describe the evolution of mechanical stresses in lithium ion (Li-ion) battery materials is extensive [12], modeling the coupled electrochemical-mechanical interaction either in bulk SPE or across the electrode-SPE interface [13] has not been considered until recently. The coupling between stress field and transport of charged species in solids has been investigated by Bucci et al. [14] who developed a model for crystalline lattices in which diffusion of multiple charged species takes place in the presence of stress, electrostatic, and chemical potential gradients. The constitutive equations, drawn from a thermodynamics framework, are suitable for an elastic medium. Natsiavas et al. [13] adopted a similar model for the description of solid electrolytes while modeling the growth of dendrites along the solid electrolyte-electrode interface. However, the implications of the coupling for a solid polymer electrolyte placed in a battery were not analyzed. A parametric study in which the electrochemical performance of the polymer electrolyte is evaluated for a range of mechanical properties is therefore performed in this study.

The properties of SPEs can be tuned by composition modifications [15], addition of nanometer-sized inclusions [16–18], or both [19]. We have assessed the response of the polymer electrolyte as a battery component by keeping the electrochemical parameters of the material fixed, while changing its mechanical properties over a range of values. The description of the coupled electrochemical-mechanical interaction is limited to the SPE. In view of this coupling, changes in material parameters alter both the electrochemical response of the electrolyte and the stress field that arises in response to the ionic redistribution. The SPE is regarded as a linear elastic isotropic material [5,13,20] in which transport of ionic species follows the Nernst-Plank's equation. The latter is modified to account for the effect exerted by pressure gradients, and the kinematics is enriched to account for the deformations induced by ionic redistribution. Following Bucci et al. [14] and Natsiavas et al. [12], the coupling between electrochemical and mechanical fields is controlled by the partial molar volume of the ionic species resulting from the dissolution of the lithium salt into the solid electrolyte. The value of the partial molar volume of $LiPF_6$ in poly(ethylene oxide) (PEO) is determined by performing molecular dynamics (MD) simulations (Section 4).

The uniform planar cell with non-porous electrodes is the simplest battery architecture. Three parallel layers of homogeneous materials (electrode—electrolyte—electrode) compose the cell. This configuration has several advantages: it facilitates casting and miniaturization of the battery [21] and makes experimental [5] and numerical investigations [22] easier. In the context of this study, this battery geometry makes the governing equations amenable to analytical investigation that allow us to show main features and implications of the model.

The steady state regime solutions for the Nernst-Planck's equation and the coupled model are compared in Section 5 for a cell not subjected to external mechanical solicitations. The results show that stresses arising in the polymer impact on the electrolyte response, as the redistribution of ions within the SPE induces a pressure gradient that alters the ionic transport. The steady state conductivity is chosen as performance indicator as it provides an indirect evaluation of the effect of different factors, such as material properties and geometrical features, on the ionic transport in the SPE. Since the latter depends on the pressure gradient, a relation is found between the stress field in the SPE and measurable quantities such as the electric current flowing through the cell and the electrostatic potential difference across the electrolyte. This makes the cell conductivity suitable for a comparison with experimental values. The results reported in Section 5 show a steady state conductivity enhancement for increasing values of the polymer Young's modulus. As this trend does not follow the trend observed at the material level [4], the reasons for the discrepancy are also discussed. The extent of the improvement relates to the geometrical features, and it can be up to 38% with respect to the electrochemical solution. The results show that the values of the stresses attained in the SPE are significant, especially because they arise from ionic redistribution only, as no externally applied loads are present. More specifically, the stresses are maximum at the electrode-electrolyte interface indicating interface detachment as the most plausible cause of battery failure. In Section 6 we focus on the response of a SPE film subjected to bending during a galvanostatic charging process. We show that the salt concentration gradient across the SPE layer can theoretically be set to zero or, at least, reduced by subjecting the film to a specific curvature. This suggests that mechanical solicitations can potentially be exploited to increase the range of current values at which the SPE film could be employed avoiding salt depletion at the electrode-electrolyte interface.

2. Model formulation

Solid polymer electrolytes in Li-ion batteries show a two-way coupling between electrochemistry and mechanics. In this section, we provide the set of balance and constitutive equations that allows the description of the coupled electrochemical-mechanical problem. The model is first formulated in terms of the electrostatic potential, positive and negative ions concentrations, and displacements. In Section 2.4 the governing equations are rephrased in a simplified form exploiting the electroneutrality assumption thus lowering the number of unknowns to three.

The formulation is expressed in a multi-dimensional notation as this paper presents the theoretical background also for a companion paper [11] that focuses on microbatteries with a trench geometry. In Sections 5 and 6, the governing equations are particularized to a one-dimensional setting, suitable for uniform planar cells.

2.1. General modeling assumptions

We focus on the description of processes taking place in the electrolyte. Current collectors and electrodes are not modeled in an

explicit manner [23–25]. The formulation, as presented, applies to binary ionic compounds that dissociates into monovalent ions only (e.g., $LiPF_6$). The following simplifying assumptions are considered:

1. the SPE is regarded as a homogeneous solid material in perfect contact with the electrodes;
2. electrical double layers—also denoted as boundary [26] or space-charge [27] layers—at the electrode-electrolyte interface [28] are not described (their thickness is usually in the order of tens to few hundreds nm for solid electrolytes according to Ref. [27] and references therein);
3. charge transfer across the electrode-electrolyte interface is continuous and side reactions are neglected in the whole cell;
4. saturation of the electrolyte is not accounted for;
5. electrodes do not undergo volume changes; and
6. the mechanical model is based on the infinitesimal strain theory.

In what follows, the subscripts Pos, Neg and SPE refer to the positive and negative electrodes and to the solid polymer electrolyte, respectively. Likewise, the corresponding domain of validity of the equations is indicated with $\boldsymbol{x} \in V_k$, where $k =$ Pos, Neg or SPE. All the field variables depend on both location $\boldsymbol{x} \in V_k$ and time $t \in [0, t_{\text{end}})$, as reported when they are introduced. The dependence on $\boldsymbol{x}$ and t will be omitted afterwards, and it will also be omitted for all the quantities derived from the field variables.

2.2. Balance equations

The dynamics of the system under consideration can be described by the following balance laws. For ionic conducting systems, the balance of charge [29] reads

$$\frac{\partial \zeta}{\partial t} + \operatorname{div} \boldsymbol{j} = 0\,, \quad \boldsymbol{x} \in V_{\text{SPE}},\ t \in [0, t_{\text{end}}), \tag{1}$$

where ζ is the charge density (electric charge per unit volume) and $\boldsymbol{j}$ is the electric current density (electric charge per unit time per unit surface). In the following, bold lower-case characters identify vectors and bold upper-case or Greek characters identify tensors.

The mass balance equation

$$\frac{\partial c_\alpha}{\partial t} + \operatorname{div} \boldsymbol{h}_\alpha = 0\,, \quad \boldsymbol{x} \in V_{\text{SPE}},\ t \in [0, t_{\text{end}}), \tag{2}$$

with $c_\alpha(\boldsymbol{x}, t)$ the molar concentration (number of moles per unit volume) and $\boldsymbol{h}_\alpha$ the mass flux (number of moles per unit time per unit surface) of species α, is written in its homogeneous form, without source term, because no chemical reactions are considered—the salt is assumed to be fully dissociated in the electrolyte.

It is assumed that a binary salt, LiX, fully dissociates in the polymer electrolyte in two ionic species: Li^+ cations and X^- anions. The charge density ζ and the electric current density $\boldsymbol{j}$ within the electrolyte are related to the ionic concentrations c_α and to the mass fluxes $\boldsymbol{h}_\alpha$ by Faraday's law of electrolysis [30]:

$$\zeta = F \sum_{\alpha = \text{Li}^+,\, \text{X}^-} z_\alpha\, c_\alpha, \quad \boldsymbol{x} \in V_{\text{SPE}},\ t \in [0, t_{\text{end}}), \tag{3a}$$

$$\boldsymbol{j} = F \sum_{\alpha = \text{Li}^+,\, \text{X}^-} z_\alpha\, \boldsymbol{h}_\alpha, \quad \boldsymbol{x} \in V_{\text{SPE}},\ t \in [0, t_{\text{end}}), \tag{3b}$$

with $F = 96485.3$ C mol^{-1} the Faraday's constant and z_α the charge number for ionic species α.

The balance of linear momentum for a solid in static equilibrium is expressed as

$$\operatorname{div} \boldsymbol{\sigma} + \boldsymbol{b}_\zeta = 0, \quad \boldsymbol{x} \in V_{\text{SPE}},\ t \in [0, t_{\text{end}}), \tag{4}$$

with $\boldsymbol{\sigma}$ (force per unit surface) the stress tensor, symmetric because of the balance of angular momentum, and $\boldsymbol{b}_\zeta$ (force per unit volume) the electrostatic forces of interaction of a charge density ζ in an electric field. Equation (4) states that electric and stress fields are related in the presence of charge densities [31]. Mechanical body forces are neglected according to Refs. [13,24,31].

Balance equations (1) and (2) represent the basis of a large number of electrochemical models [32–34] employed for the description of batteries with non-porous electrodes. The contribution of mechanical deformations is incorporated in recent studies with the equilibrium equation (4) added to the system of balance equations [13,14]. Other approaches in which more general sets of equations were considered in place of (1) are described in Refs. [26,27,31,35].

The balance equations (1)–(4) refer to the reference undeformed configuration according to the infinitesimal strain theory: geometry and constitutive properties of the electrodes and the SPE do not change during any of the processes under investigation.

2.3. Constitutive equations

The evolution of primary or derived fields and their couplings are described through constitutive equations. The diffusion coefficients, partial molar volume, and mechanical properties of the solid polymer electrolyte are assumed to be constant.

Generalized Nernst-Plank's equation. The flux of the ionic species in the solid electrolyte is described through the Nernst-Plank's equation [32] modified according to [13,14] to account for the effect of stresses:

$$\begin{aligned} &\boldsymbol{h}_\alpha = -\, D_\alpha\, \nabla c_\alpha \;-\; \frac{z_\alpha F}{RT}\, D_\alpha\, c_\alpha\, \nabla \phi - \frac{D_\alpha}{RT}\, \Omega_\alpha\, c_\alpha\, \nabla p, \\ &\alpha = \text{Li}^+,\ \text{X}^-, \quad \boldsymbol{x} \in V_{\text{SPE}},\ t \in [0, t_{\text{end}}), \end{aligned} \tag{5}$$

where $R = 8.31447$ J K^{-1} mol^{-1} is the ideal gas constant, T is the absolute temperature, taken as the room temperature ($T = 298.15$ K) in this study, D_α and Ω_α are the ionic diffusivity (m^2 s^{-1}) and the partial molar volume (m^3 mol^{-1}) of the ionic species α, respectively. The electrostatic potential $\phi(\boldsymbol{x}, t)$ and the pressure p are defined in the next paragraphs. The three terms on the right-hand side represent (from left to right) the contribution of diffusion, migration, and pressure-induced mass flux. Convection is usually negligible in polymer (not just solid) electrolytes [3,36] and is often not included in models for crystalline [37] and amorphous [22] solid electrolytes. In case of neutral species, the second term on the right-hand side in (5) vanishes and the usual model for diffusion of species in a stressed lattice is recovered [38].

Stress-strain relation. The strain tensor is defined as

$$\boldsymbol{\varepsilon} = \frac{1}{2}(\nabla \boldsymbol{u} + \nabla \boldsymbol{u}^T), \quad \boldsymbol{x} \in V_{\text{SPE}},\ t \in [0, t_{\text{end}}), \tag{6}$$

with $\boldsymbol{u}(\boldsymbol{x}, t)$ the displacement vector. The strain tensor $\boldsymbol{\varepsilon}$ can be additively decomposed into two contributions:

$$\boldsymbol{\varepsilon} = \boldsymbol{\varepsilon}^{\text{el}} + \sum_{\alpha = \text{Li}^+, \text{X}^-} \frac{\Omega_\alpha}{3}(c_\alpha - c_\alpha^0)\, \mathbf{1}, \quad \boldsymbol{x} \in V_{\text{SPE}},\ t \in [0, t_{\text{end}}),$$

where $\boldsymbol{\varepsilon}^{\text{el}}$ represents the elastic deformation, and the second term on the right-hand side represents the inelastic chemical

deformation due to concentration redistribution with respect to a reference molar concentration c_α^0 for each ionic species α. The identity tensor is denoted with $\mathbf{1}$.

A linear elastic constitutive model is used for the mechanical description of the SPE [20]. This choice is valid for deformations up to approximately 10%. More advanced constitutive models would be needed for the investigation of the polymer response under extreme conditions, provided that experimental data are available for their calibration. The stress tensor $\boldsymbol{\sigma}$ within the solid electrolyte is expressed as the sum of its deviatoric component and pressure

$$p = -\frac{\mathrm{tr}\,\boldsymbol{\sigma}}{3} = -K\,\mathrm{tr}\boldsymbol{\varepsilon} + K \sum_{\alpha=\mathrm{Li}^+,\,\mathrm{X}^-} \Omega_\alpha\,(c_\alpha - c_\alpha^0), \quad \boldsymbol{x}\in V_{\mathrm{SPE}},\ t\in[0,t_{\mathrm{end}}) \tag{7}$$

as in

$$\boldsymbol{\sigma} = 2G\,\mathrm{dev}\boldsymbol{\varepsilon} - p\mathbf{1}, \quad \boldsymbol{x}\in V_{\mathrm{SPE}},\ t\in[0,t_{\mathrm{end}}), \tag{8}$$

where the trace of a tensor $\boldsymbol{A}$ is defined as $\mathrm{tr}\,\boldsymbol{A} = \sum_i A_{ii}$ and the deviatoric component of the same tensor corresponds to the difference $\mathrm{dev}\,\boldsymbol{A} = \boldsymbol{A} - \mathrm{tr}\,\boldsymbol{A}/3\,\mathbf{1}$.

The constants G and K represent the shear and the bulk moduli, respectively. The stress field is affected by the presence of ions only through the last term in (7), which is dealt with as a thermal deformation component [38,39]. Similar to Bucci et al. [14] the effects of the ionic concentration and electrostatic forces on the mechanical properties of the material have been neglected.

2.4. Electroneutrality assumption

The problem is formulated in terms of the field variables ϕ, c_{Li^+}, c_{X^-} and $\boldsymbol{u}$ through balance equations (1)–(4) and constitutive equations (5), (7) and (8). Nevertheless, relations (3) make (1) and (2) redundant because if c_i and $\boldsymbol{h}_i$ satisfy (2), also (1) is satisfied due to (3), and thus another equation needs to be introduced to make the problem solvable. Following a standard approach, we assume that electroneutrality holds within the electrolyte [30]:

$$F \sum_{\alpha=\mathrm{Li}^+,\,\mathrm{X}^-} z_\alpha\,c_\alpha = 0, \quad \boldsymbol{x}\in V_{\mathrm{SPE}},\ t\in[0,t_{\mathrm{end}}). \tag{9}$$

This equation states that, over the length scale considered, no net charge can be detected in the electrolyte at any moment of time. Condition (9) is widely used in the literature (e.g., [23,30,32,36,40]), as it provides the constraint required to make the system of equations solvable and allows to reduce the number of unknowns. In fact, for a binary salt that dissociates into monovalent ionic species ($z_{\mathrm{Li}^+}=1$ and $z_{\mathrm{X}^-}=-1$) it follows that

$$c_{\mathrm{Li}^+}(\boldsymbol{x},t) = c_{\mathrm{X}^-}(\boldsymbol{x},t) = c(\boldsymbol{x},t), \quad \boldsymbol{x}\in V_{\mathrm{SPE}},\ t\in[0,t_{\mathrm{end}}). \tag{10}$$

The balance and constitutive equations listed in Sections 2.2 and 2.3 can be rephrased to reformulate the original problem in terms of the field variables ϕ, $\boldsymbol{u}$ and the newly introduced c. Alternative approaches not considered in this paper have been applied to the modeling of ionic conductors moving form a subset of Maxwell's equations [24–27,37].

The first term on the left-hand side of (1) vanishes because of the electroneutrality condition: being the charge density

$$\zeta = 0, \quad \boldsymbol{x}\in V_{\mathrm{SPE}},\ t\in[0,t_{\mathrm{end}}), \tag{11}$$

equation (1) results in

$$\mathrm{div}\boldsymbol{j} = 0, \quad \boldsymbol{x}\in V_{\mathrm{SPE}},\ t\in[0,t_{\mathrm{end}}). \tag{12}$$

The electric current density appearing in (12) can be expressed as a function of the ionic concentration, electrostatic potential and pressure gradients as

$$\boldsymbol{j} = \gamma_c\,\nabla c - \gamma_\phi\,c\,\nabla\phi + \gamma_p\,c\,\nabla p, \quad \boldsymbol{x}\in V_{\mathrm{SPE}},\ t\in[0,t_{\mathrm{end}}), \tag{13}$$

having collected the material constants into the coefficients

$$\gamma_c = F\,(D_{\mathrm{X}^-} - D_{\mathrm{Li}^+}), \tag{14a}$$

$$\gamma_\phi = \frac{F^2}{RT}\,(D_{\mathrm{Li}^+} + D_{\mathrm{X}^-}), \tag{14b}$$

$$\gamma_p = F\,\frac{D_{\mathrm{X}^-}}{RT}\,\Omega\left(\frac{\Omega_{\mathrm{X}^-}}{\Omega} - \frac{D_{\mathrm{Li}^+}}{D_{\mathrm{X}^-}}\left(1 - \frac{\Omega_{\mathrm{X}^-}}{\Omega}\right)\right), \tag{14c}$$

and defining the combined partial molar volume as

$$\Omega = \Omega_{\mathrm{Li}^+} + \Omega_{\mathrm{X}^-}\,. \tag{15}$$

By following the approach detailed in Refs. [23,32], the mass balance equation (2) of ionic species Li^+ and X^- are multiplied respectively by D_{X^-} and D_{Li^+}. After summing them up and dividing the resulting equation by $D_{\mathrm{Li}^+} + D_{\mathrm{X}^-}$ one is left with

$$\frac{\partial c}{\partial t} + \mathrm{div}\boldsymbol{h} = 0, \quad \boldsymbol{x}\in V_{\mathrm{SPE}},\ t\in[0,t_{\mathrm{end}}), \tag{16}$$

where the apparent mass flux

$$\boldsymbol{h} = \frac{D_{\mathrm{X}^-}\,\boldsymbol{h}_{\mathrm{Li}^+} + D_{\mathrm{Li}^+}\,\boldsymbol{h}_{\mathrm{X}^-}}{D_{\mathrm{Li}^+} + D_{\mathrm{X}^-}}, \quad \boldsymbol{x}\in V_{\mathrm{SPE}},\ t\in[0,t_{\mathrm{end}}), \tag{17}$$

can be expressed in terms of concentration (c) and pressure and concentration gradients (∇p and ∇c, respectively) yielding

$$\boldsymbol{h} = -D\,\nabla c - \frac{1}{2}\,\frac{D}{RT}\,\Omega\,c\,\nabla p, \quad \boldsymbol{x}\in V_{\mathrm{SPE}},\ t\in[0,t_{\mathrm{end}}). \tag{18}$$

In this equation, the apparent diffusivity is defined as

$$D = \frac{2\,D_{\mathrm{Li}^+}\,D_{\mathrm{X}^-}}{D_{\mathrm{Li}^+} + D_{\mathrm{X}^-}}\,, \tag{19}$$

and the volumetric term of the stress tensor

$$p = -K\,\mathrm{tr}\boldsymbol{\varepsilon} + K\,\Omega\,(c - c^0), \quad \boldsymbol{x}\in V_{\mathrm{SPE}},\ t\in[0,t_{\mathrm{end}}). \tag{20}$$

Finally, the electroneutrality assumption allows to uncouple mechanical and electric fields in the mechanical equilibrium equation (4). Since the charge density ζ equals zero (11) no electrostatic forces of interactions arise in the electrolyte, and term $\boldsymbol{b}_\zeta$ equals zero as well, thus making the equilibrium equation (4) homogeneous. A detailed discussion about the role of the electroneutrality assumption on the electrostatic body forces can be found in Ref. [31]. Bucci et al. [14] highlight that the so-called Maxwell stress is sometimes added to the mechanical stress (8), in substitution of the body forces $\boldsymbol{b}_\zeta$ in (4). This is not the case here. Because of the arguments just exposed, the contribution of the Maxwell stress is assumed to be negligible, in agreement with Refs. [13,14]. An a posteriori verification of this assumption is reported in Appendix A. The last of the balance laws, the balance of linear momentum (4), reduces to

$$\mathrm{div}\boldsymbol{\sigma} = 0, \quad \boldsymbol{x}\in V_{\mathrm{SPE}},\ t\in[0,t_{\mathrm{end}}). \tag{21}$$

To summarize, the electroneutrality condition (9) allows to reformulate the problem in terms of ϕ, c and $\boldsymbol{u}$, by replacing the set of balance and constitutive equations (1)–(5) by (12), (13), (16), (18) and (21). Provided that the pressure definition (7) is replaced by (20), the stress definition (8) remains valid. The problem can now be solved for a suitable set of boundary and initial conditions.

Electrochemical-mechanical coupling is due to the redistribution of ionic species that causes swelling and shrinkage of the SPE. Models accounting for different electrochemical-mechanical couplings have been reported for solid electrolyte with a single mobile ionic species. Braun et al. [27] developed their models starting from thermodynamic principles in which pressure is related to constituents concentration (expressed in terms of "number density") and electric field. From the mechanical perspective the electrolyte was modeled as an incompressible fluid in agreement with the model originally developed by Dreyer et al. [26] for liquid electrolytes. The models reported in Refs. [26,27] are characterized by a higher level of complexity compared to the adopted model: the adoption of combined analytical-numerical techniques is necessary even to tackle one-dimensional equilibrium problems (characterized by vanishing time derivative and vanishing fluxes). Their main goal is to provide a description of the boundary layers that form at the electrode-electrolyte interface, whose representation is out of the scope of this study. Apart from the boundary layer description, the adopted model is different because it accounts for a non-uniform distribution of pressure even for vanishing free charges (11) and in absence of convection. Moreover, our model accounts for shear stresses and it is not restricted to incompressible materials.

3. Governing equations and interface conditions

The equations that govern the problem together with the interface conditions that follow from the electroneutrality assumption (9) are summarized in this section.

A coupled problem, formulated in terms of the field variables ϕ, c and $\boldsymbol{u}$, can be formulated for the electrolyte domain V_{SPE} by substituting (8), (13), (18) and (20) into the balance equations (12), (16) and (21):

$$\begin{aligned}&\mathrm{div}(\,\gamma_c\nabla c - \gamma_\phi\, c\,\nabla\phi + \gamma_p\, c\,\nabla p) = 0,\\ &\boldsymbol{x}\in V_{\mathrm{SPE}},\ t\in[0,t_{\mathrm{end}}),\end{aligned} \tag{22a}$$

$$\begin{aligned}&\frac{\partial c}{\partial t} + \mathrm{div}\Big(-D\,\nabla c - \frac{1}{2}\frac{D}{RT}\,\Omega\, c\,\nabla p\Big) = 0,\\ &\boldsymbol{x}\in V_{\mathrm{SPE}},\ t\in[0,t_{\mathrm{end}}),\end{aligned} \tag{22b}$$

$$\begin{aligned}&\mathrm{div}(2G\,\mathrm{dev}\boldsymbol{\varepsilon} + K\,\mathrm{tr}\boldsymbol{\varepsilon}\,\mathbf{1} - K\Omega\,(c-c^0)\mathbf{1}\,) = 0,\\ &\boldsymbol{x}\in V_{\mathrm{SPE}},\ t\in[0,t_{\mathrm{end}}).\end{aligned} \tag{22c}$$

Equation (22) clearly shows that the electrochemical-mechanical coupling exclusively depends on the combined partial molar volume Ω, and that for $\Omega = 0$ the formulation used in Ref. [32] is recovered (i.e. the ionic conduction is independent of the stress field)—Section 4.1 is devoted to the description of the procedure that leads to the identification of Ω for $LiPF_6$ dissolved in two solid polymer electrolytes.

The electric charge transferred across the electrode-electrolyte interface during battery operations is related to the amount of Li-ions exchanged through

$$\begin{aligned}&\boldsymbol{j}\cdot\boldsymbol{n} = F\boldsymbol{h}_{\mathrm{Li}^+}\cdot\boldsymbol{n},\\ &\boldsymbol{x}\in(\partial V_{\mathrm{Pos}}\cap\partial V_{\mathrm{SPE}})\cup(\partial V_{\mathrm{Neg}}\cap\partial V_{\mathrm{SPE}}),\ t\in[0,t_{\mathrm{end}}),\end{aligned} \tag{23}$$

where ∂V denotes the boundary of domain V as shown in Fig. 2. Recalling that only Li-ions cross the electrode-electrolyte interface, the homogeneous boundary condition

$$\boldsymbol{h}_{\mathrm{X}^-}\cdot\boldsymbol{n} = 0, \quad \boldsymbol{x}\in(\partial V_{\mathrm{Pos}}\cap\partial V_{\mathrm{SPE}})\cup(\partial V_{\mathrm{Neg}}\cap\partial V_{\mathrm{SPE}}),\ t\in[0,t_{\mathrm{end}}) \tag{24}$$

are applied to the anionic mass flux.

Combining (23) and (24) by following the procedure applied to the mass balance equation (2), the interface conditions

$$\begin{aligned}&\boldsymbol{h}\cdot\boldsymbol{n} = \frac{1}{F}\frac{D_{\mathrm{X}^-}}{D_{\mathrm{Li}^+}+D_{\mathrm{X}^-}}\,\boldsymbol{j}\cdot\boldsymbol{n}\,,\\ &\boldsymbol{x}\in(\partial V_{\mathrm{Pos}}\cap\partial V_{\mathrm{SPE}})\cup(\partial V_{\mathrm{Neg}}\cap\partial V_{\mathrm{SPE}}),\ t\in[0,t_{\mathrm{end}})\end{aligned} \tag{25}$$

for the apparent mass flux are obtained. Since the field variables c_{Li^+} and c_{X^-} are replaced by c following the arguments provided in Section 2.4, only the relationship (25) between apparent mass flux and electric current density will be used in the following sections.

Boundary conditions are described in Section 5 where details about the cell geometry are provided.

4. Material parameters

The solid polymer electrolyte is a PEO with $LiPF_6$ salt with ionic diffusivity values $D_{\mathrm{Li}^+} = 2.5\times10^{-13}\ \mathrm{m^2\ s^{-1}}$ and $D_{\mathrm{PF}_6^-} = 3.0\times10^{-13}\ \mathrm{m^2\ s^{-1}}$ as from Zadin and Brandell [32]. No electrochemical parameters other than those just listed enter the model, and these values are used in all the analyses discussed in Section 5. Different values of the Young's modulus (E = 5, 50, 140 and 500 MPa) are considered to investigate its impact on the battery cell performance for a fixed set of electrochemical properties. This range spans over two decades, exceeding the interval of variability of the elastic properties of inorganic solid electrolytes [41]. The values are selected according to experimental studies carried either on PEO [8,9,18] or poly(propylene glycol) diacrylate (PPGDA) [42,43] which have chemical structure similarities and show similar properties [44]. The value of the Poisson's ratio ($\nu = 0.24$) was experimentally determined for PEO in Ref. [9].

Assuming it is possible to extrapolate a Young's modulus-diffusivity relationship from the stiffness-conductivity curve reported in Fig. 1, it appears that the error we commit by keeping the diffusivity fixed over the explored range of Young's modulus values (5–500 MPa) is limited, given that the electrochemical properties

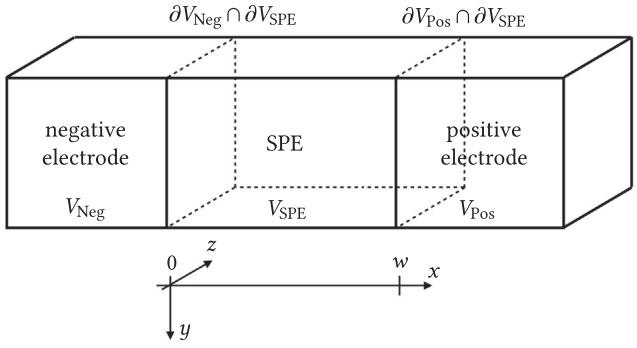

Fig. 2. Schematic of a uniform planar cell.

(conductivity/diffusivity) span over seven decades. The interval of Young's modulus values explored in this study corresponds to the lowest values of conductivity/diffusivity reported in Fig. 1; it therefore follows that concentration gradients are pronounced. The results showed in Section 5.1 suggest that limited modifications of the mechanical properties lead to a non-negligible benefit in this range of properties. In addition, experimental studies by Snyder et al. [15,45] show a large dispersion of conductivity values for polymer electrolytes characterized by mechanical properties similar to those considered here. This makes it hard to choose a Young's modulus-diffusivity relationship without introducing a significant level of arbitrariness in the model. For these reasons, the assumption of a fixed diffusivity is adopted with the aim of isolating the effect that a modification of the mechanical properties has on the overall electrochemical performance (through the electrochemical-mechanical coupling), quantified in terms of steady state conductivity and concentration gradient extent.

4.1. Partial molar volume

The partial molar volume of substance k [46],

$$\Omega_k = \left(\frac{\partial V}{\partial n_k}\right)\Big|_{p,T}, \tag{26}$$

is the contribution to the volume that the substance makes when it is part of a mixture and is a function of the volume V of the mixture and the number n_k of moles of species k in the mixture. The definition is valid under constant pressure and temperature.

By considering the solid polymer electrolyte and the $LiPF_6$ salt as a mixture, and assuming an approximately piecewise linear dependence of the volume of the mixture on the salt, the partial molar volume of $LiPF_6$,

$$\Omega_{LiPF_6} \cong \frac{\delta V}{\delta n_{LiPF_6}}\Big|_{p,T}, \tag{27}$$

is expressed as the ratio between the volume change δV of the system composed by the polymer and the salt in response to a change δn_{LiPF_6} in the number of $LiPF_6$ moles at constant pressure and temperature—throughout this section pressure and temperature are always considered as constants. If a mixture with no salt molecules—a pure polymer—occupying a volume V_0 is chosen as a reference, equation (27) can be rephrased as

$$\Omega_{LiPF_6} = \frac{1}{c_{LiPF_6}}\left(1 - \frac{V_0}{V}\right), \tag{28}$$

provided that the molar concentration

$$c_{LiPF_6} = \frac{n_{LiPF_6}}{V} \tag{29}$$

of $LiPF_6$ in the mixture is introduced, where V is the volume of the mixture containing n_{LiPF_6} moles of salt. Equation (28) holds true for $c_{LiPF_6} > 0$, being $n_{LiPF_6} \geq 0$.

The quantity defined in (28) is usually called apparent molar volume [47] and, in view of the use of the volume V_0 of the pure polymer rather than the actual volume of the polymer in solution, it is sometimes considered an artificial quantity. The standard partial molar volume is preferred for many applications as it is formally more correct since it corresponds to the apparent molar volume in the limit of infinite dilute solution ($c_{LiPF_6} \to 0$). Both theoretical and empirical relations linking these two quantities can be found in the literature; due to the lack of available data, definition (28) will be used hereafter for the partial molar volume, following the approach pursued by Zhang et al. [38]. For a deeper discussion on the topic the reader is referred to the review by Marcus and Hefter [47].

If the density ρ of the mixture is known for a specific $LiPF_6$ content, the ratio V/V_0 can be determined through

$$\frac{V}{V_0} = \frac{M_{polymer} + x_{LiPF_6} M_{LiPF_6}}{M_{polymer}} \frac{\rho_0}{\rho}, \tag{30}$$

where $M_{polymer}$ and $M_{LiPF_6} = 151.90\ g\ mol^{-1}$ represent the molar masses of the polymer and the salt, respectively, x_{LiPF_6} represents the mole fraction of the salt, and ρ_0 is the density of the pure polymer. The polymers considered in this study are PEO, polymer molecule $C_{456}H_{914}O_{229}$, and crosslinked PPGDA, unit cell $C_{168}H_{288}O_{64}$, with molar masses $M_{C_{456}H_{914}O_{229}} = 10062.10\ g\ mol^{-1}$ and $M_{C_{168}H_{288}O_{64}} = 3333.06\ g\ mol^{-1}$, respectively.

The full set of data for the partial molar volume evaluation of the PPGDA polymer electrolyte through (28)–(30) has been determined by MD simulations and is available in Ref. [44]. The analogous set of parameters for the PEO polymer electrolyte is determined performing MD simulations according to the procedure detailed in Appendix B. The parameters of interest for both polymers are summarized in Table 1.

By making use of the values listed in Table 1 and substituting them into (30) the volume change of the mixture normalized by the current volume $1 - V_0/V$ can be evaluated (Fig. 3 shows a plot of this quantity against the molar concentration c_{LiPF_6}). The slopes of the continuum lines in the plot, obtained via linear least squares fitting of the data, provide an estimate of the partial molar volume of the $LiPF_6$ in PEO ($\Omega_{LiPF_6} = 1.150 \times 10^{-4}\ m^3\ mol^{-1}$) and PPGDA ($\Omega_{LiPF_6} = 1.461 \times 10^{-4}\ m^3\ mol^{-1}$) as from (28).

It should be noted that the partial molar volume Ω_{LiPF_6} in (28) is not formally equivalent to the combined partial molar volume Ω in (15). While the latter represents the sum of the partial molar volumes of each ionic species from the dissociation of $LiPF_6$ into Li^+ and PF_6^-, the former is representative of the volume change of the mixture when $LiPF_6$ is introduced, as a whole, into a polymer electrolyte. It has been discussed in Ref. [44] that the dissociation of $LiPF_6$ in the MD simulations was only partial, and thus the response of the mixture depended on both bonded $LiPF_6$ and dissociated Li^+

Table 1
$LiPF_6$/PPGDA and $LiPF_6$/PEO density vs $LiPF_6$ concentration at 1 atm and 300 K.

	unit cell/single polymer molecule	Li:O	x_{LiPF_6}	c_{LiPF_6} (mol dm^{-3})	ρ (g cm^{-3})
PPGDA[a]	$C_{168}H_{288}O_{64}$	0	0.0	0.00	1.167
		1:42	1.5	0.48	1.152
		1:21	3.0	0.92	1.152
PEO	$C_{456}H_{914}O_{229}$	0	0.0	0.00	1.155
		1:40	5.7	0.60	1.157
		1:20	11.4	1.13	1.180

[a] Data referring to PPGDA taken form Ref. [44].

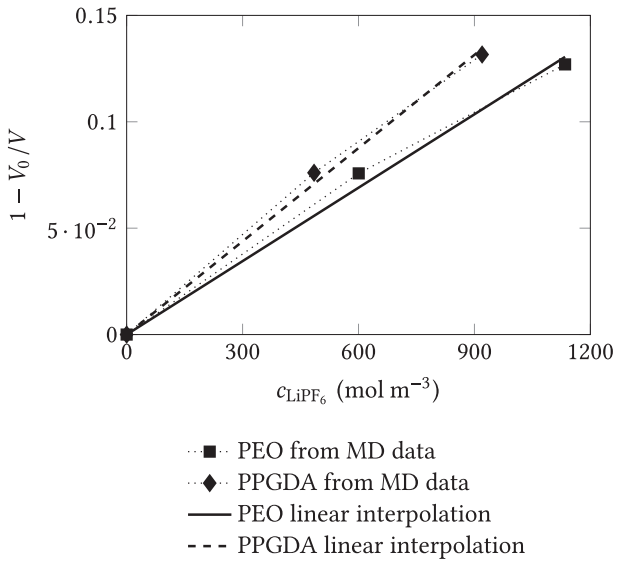

Fig. 3. Partial molar volume of $LiPF_6$ in PEO and PPGDA solid electrolytes.

and PF_6^-. The data obtained from the MD simulations represent the average response of the system to multiple (concurrent) phenomena, similar to the values of Ω_{LiPF_6} obtained from them.

Fig. 3 shows that the partial molar volume is constant over the range of salt concentration values explored by means of the MD simulations. This observation is in agreement with experimental studies [36,40,48] that report constant values of the partial molar volume even for higher salt content—the partial molar volume of $LiPF_6$ in a copolymer of ethylene oxide and propylene oxide (EOPO) [36] and in a ethylene carbonate (EC)/ethyl methyl carbonate (EMC) [48] mixtures was determined to be constant for salt concentration up to 2000 mol m^{-3}.

The estimates of Ω_{LiPF_6} provide a sound indication of the range of values that should be explored. The analyses are performed using $\Omega = 1.1 \times 10^{-4}$ m^3 mol^{-1} and $\Omega = 1.5 \times 10^{-4}$ m^3 mol^{-1}, representing the lower and upper bounds of the values obtained from Fig. 3. It needs to be pointed out that these values fall in the range of literature values for battery electrolytes. A standard partial molar volume equal to 6.24×10^{-5} m^3 mol^{-1} has been experimentally determined for $LiPF_6$ in propylene carbonate (PC) at 40 °C by Naejus et al. [49], and similar values (up to 7.42×10^{-5} m^3 mol^{-1}) are reported for different lithium salts in ethylene carbonate (EC) and PC at 25 °C [47]. Partial molar volume equal to 6.5×10^{-5} m^3 mol^{-1} [40] and 5.9×10^{-5} m^3 mol^{-1} [48] are provided for $LiPF_6$ in EC/diethylene carbonate (DEC)/poly(methyl methacrylate) (PMMA) and EC/ethyl methyl carbonate (EMC) mixtures, respectively. Ma et al. [50] estimated a partial molar volume equal to 3.6×10^{-5} m^3 mol^{-1} for sodium trifluoromethanesulfonate ($NaCF_3SO_3$) in PEO, while Georen and Lindbergh [36] determined the partial molar volume of LiTFSI in EOPO to be 1.42×10^{-4} m^3 mol^{-1}. Finally, a partial molar volume $\Omega \approx 6.667 \times 10^{-4}$ m^3 mol^{-1} was used by Natsiavas et al. [13] in numerical simulations performed on Li^+ ions dissolved in a solid-state lithium phosphorus oxynitride (LiPON) electrolyte—unfortunately, no references were reported regarding the origin of this value. The lower bound determined with our MD simulations for the partial molar volume lies in a range between 0.8 and 3 times the experimentally determined values listed above, while our upper bound is about 4 times smaller compared to the maximum value reported in the literature (6.667×10^{-4} m^3 mol^{-1} [13]). Given that the impact of the mechanical contribution on our results is proportional to both the partial molar volume of the salt and the Young's modulus of the polymer, we can consider the just mentioned variability to be absorbed within the wide range considered for the Young's modulus (two decades) in Section 5.

According to definition (26) there are no restriction on the values of Ω_{Li^+} and $\Omega_{PF_6^-}$, and these quantities could even be negative [46]—which is the case for other contexts, e.g., vacancies diffusing in an aluminum lattice [51]. As a consequence, the ratio $\Omega_{PF_6^-}/\Omega$ in (14c) could also be negative. However, since local charge separation is prevented in agreement with (9), the ratio $\Omega_{PF_6^-}/\Omega$ is here interpreted as the contribution of the negative ions to the overall volume change; being the combined partial molar volume Ω positive, the ratio $\Omega_{PF_6^-}/\Omega$ is assumed to be positive as well. A first estimate of the contribution of each ionic species to the combined partial molar volume Ω can be based on the ionic radii of the two ions: values of 0.076 nm and 0.254 nm are reported for the ionic radii of Li^+ and PF_6^- by Ue [52]. By assuming that the contribution of each ionic species to the SPE volume expansion is proportional to the volume it occupies, the ratio $\Omega_{Li^+}/\Omega_{PF_6^-} \cong 1/37$ should be used, thus leading to $\Omega_{PF_6^-}/\Omega \cong 37/38$ in (14c). This indicates that the volumetric deformation of the hosting polymer due to concentration redistribution is basically ascribed to the PF_6^- anion.

Although the results discussed in Section 5 refer to $\Omega_{PF_6^-}/\Omega = 37/38$, a series of analyses was performed for a wider range of values. Those results are not reported here because differences were appreciable for the electrostatic potential profiles (20% at most) when $\Omega_{PF_6^-}/\Omega = 1/2$, while all the results become indistinguishable for $\Omega_{PF_6^-}/\Omega \in [9/10, 1]$. The combined partial molar volume Ω will be simply identified as partial molar volume from now on.

5. Uniform planar cell: No externally induced deformations

A uniform planar cell with non-porous electrodes is considered. Three parallel layers of homogeneous material make up the battery represented in Fig. 2. It is assumed that expansion of the cell is prevented by the external coating and that the SPE perfectly adheres to the electrodes. The latter are regarded as non-deformable and infinitely rigid. The first assumption is consistent with the choice of limiting the modeling to the SPE, while the second is motivated by the difference in mechanical properties with respect to the polymer—using for instance lithium cobalt oxide ($LiCoO_2$) and graphite (C_6) as in Ref. [32] would imply characteristic Young's modulus values equal to 150 GPa [53–55] and 25 GPa [56,57], respectively, largely exceeding the maximum value used for the SPE in this study.

Assuming that the extension of the cell in the y and z directions is sufficiently large to consider boundary effects negligible, the components of the electric current density and the mass fluxes in these directions can be neglected [23]. All processes therefore occur along the x direction only, allowing the reformulation of the governing equations in Section 3 in a simplified one-dimensional setting. Analytical solutions for the field variables can be obtained, providing a reference for numerical implementation (an analytical solution for a one-dimensional problem limited to chemo-mechanical interaction can be found in [58], please note that also boundary conditions differ from those considered here). Nevertheless, the interest in this particular battery architecture goes beyond the ease of modeling. Thin-film all-solid-state batteries either with polymer [21] or inorganic [22] electrolytes are commonly cast in such a configuration. Since inorganic electrolytes

(e.g., LiPON) were recently studied with governing equations similar to those considered in this study, accounting [13] or not [59] for the mechanical contribution, our approach applies to their description as well, provided that a suitable set of material parameters is used. For the sake of readability, index x will be omitted throughout this section.

This particular configuration allows to rephrase (13), (18) and (20) in a one-dimensional setting as

$$j = \gamma_c \frac{\partial c}{\partial x} - \gamma_\phi\, c\, \frac{\partial \phi_{\mathrm{SPE}}}{\partial x} + \gamma_p\, c\, \frac{\partial p}{\partial x}, \quad x \in [0, w],\ t \in [0, t_{\mathrm{end}}), \tag{31a}$$

$$h = -D\, \frac{\partial c}{\partial x} - \frac{1}{2}\, \frac{D}{RT}\, \Omega\, c\, \frac{\partial p}{\partial x}, \quad x \in [0, w],\ t \in [0, t_{\mathrm{end}}), \tag{31b}$$

with w the width of the SPE as from Fig. 2.

Assuming that no external loads are applied on the cell and that the extension in the y and z directions is sufficiently large, both the displacements and the deformations along the y and z directions are null. The strain tensor (6) reduces to

$$\varepsilon = \frac{\partial u}{\partial x}, \quad x \in [0, w],\ t \in [0, t_{\mathrm{end}}), \tag{32}$$

while three stress components are left according to definition (8):

$$\sigma_{xx} = \frac{E}{1-2\nu}\left(\frac{1-\nu}{1+\nu}\,\varepsilon - \frac{\Omega}{3}\left(c - c^0\right)\right), \quad x \in [0, w],\ t \in [0, t_{\mathrm{end}}), \tag{33a}$$

$$\sigma_{yy} = \sigma_{zz} = \frac{E}{1-2\nu}\left(\frac{\nu}{1+\nu}\varepsilon - \frac{\Omega}{3}\left(c - c^0\right)\right), \quad x \in [0, w],\ t \in [0, t_{\mathrm{end}}). \tag{33b}$$

This should not confuse the reader, the absence of deformation in the transverse y and z directions does not imply that the corresponding stress components are zero as well. The redistribution of ionic concentration c would cause expansion or contraction in a body free to deform, but it induces stresses if the deformation is impeded, which is what happens in this case. In a one-dimensional setting, equation (20) reads

$$p = \frac{E}{3\,(1-2\,\nu)}(\Omega\,(c - c^0) - \varepsilon), \quad x \in [0, w],\ t \in [0, t_{\mathrm{end}}), \tag{34}$$

and the equilibrium equation (22c) provides the relation

$$\frac{\partial \varepsilon}{\partial x} = \frac{1+\nu}{1-\nu}\,\frac{\Omega}{3}\,\frac{\partial c}{\partial x}, \quad x \in [0, w],\ t \in [0, t_{\mathrm{end}}) \tag{35}$$

between the deformation ε and the concentration c. Substitution of (34) into (31b) together with (35) leads to

$$h = -\left(D + \alpha\, \frac{1}{2}\, \frac{D}{RT}\, \Omega\, c\right)\frac{\partial c}{\partial x}, \quad x \in [0, w],\ t \in [0, t_{\mathrm{end}}), \tag{36}$$

with

$$\alpha = \frac{2}{9}\,\frac{E\Omega}{1-\nu}, \tag{37}$$

and E and ν the Young's modulus and the Poisson's ratio of the SPE, respectively.

Equation (36) expresses the one-dimensional governing equation of the apparent mass flux as a function of the ionic concentration only. Similar manipulations allowed Zhang et al. [38] and Woodford et al. [60] to express the stress-diffusion coupling in intercalation electrode particles as a concentration-dependent diffusivity (terms between brackets in (36)). Equations (36)-(37) are indeed equivalent to (37) in Ref. [38] and (1–2) in Ref. [60], the only difference is due to the factor 1/2 in (36), introduced here because of definitions (18) and (19). If the mechanical stress contribution is omitted (either $E \approx 0$ or $\Omega \approx 0$) Fick's first law is recovered. Following similar arguments, the one-dimensional electric current density (31a) is rewritten as

$$j = (\gamma_c + \alpha\, \gamma_p\, c)\frac{\partial c}{\partial x} - \gamma_\phi\, c\, \frac{\partial \phi}{\partial x}, \quad x \in [0, w],\ t \in [0, t_{\mathrm{end}}). \tag{38}$$

The one-dimensional version of (1) reads

$$\frac{\partial j}{\partial x} = 0, \quad x \in [0, w],\ t \in [0, t_{\mathrm{end}}), \tag{39}$$

which implies that the electric current density is uniform within the SPE. When a galvanostatic process is considered, the assigned electric current can be applied at the boundary of the SPE, assuming that no capacitive effects take place at the electrodes-SPE interface. With the negative electrode selected as the reference electrode, the boundary conditions

$$\phi(0, t) = 0, \quad t \in [0, t_{\mathrm{end}}) \text{ and} \tag{40a}$$

$$j(w, t) = -j_{\mathrm{bc}}, \quad t \in [0, t_{\mathrm{end}}) \tag{40b}$$

are enforced. The value of the current density j_{bc}, assigned and constant during the charging process, is set to 10 A m^{-2}, the same value used in Ref. [32]. Charge and discharge only differ by the sign in (40b): all plots that follow would be presented flipped from right to left for the discharge case. The boundary conditions

$$h(0, t) = h(w, t) = -\frac{1}{F}\,\frac{D_{\mathrm{PF_6^-}}}{D_{\mathrm{Li^+}} + D_{\mathrm{PF_6^-}}}\, j_{\mathrm{bc}}, \quad t \in [0, t_{\mathrm{end}}) \tag{41}$$

apply to the mass conservation equation according to (25). The minus signs appearing in (40b) and (41) indicate that both electric current and mass flux move from the positive electrode towards the negative electrode in agreement with Fig. 2. The expansion of the electrolyte is prevented at the boundaries by enforcing

$$u(0, t) = u(w, t) = 0, \quad t \in [0, t_{\mathrm{end}}). \tag{42}$$

Equation (42) does not imply that displacements are identically equal to zero in the entire domain $[0, w]$, as the coupling between displacements and concentrations (35) makes u non-uniform for a non-uniform distribution of c, as shown in Fig. 5.

The initial condition

$$c(x, 0) = c^0, \quad x \in [0,\ w], \tag{43}$$

with $c^0 = 1500$ mol m^{-3} [32], ensures the uniqueness of the solution of the mass conservation equation—with this condition, definition (20) implies that the SPE is in a stress-free state in the initial (undeformed) configuration.

5.1. Results and discussion

This section is dedicated to the steady state configuration, i.e., all quantities are independent of time. For uniform planar cells (and only for this specific battery architecture as discussed in a companion paper [11]), this configuration allows to obtain the maximum ionic concentration gradient in the SPE and the largest deviation of c from c^0. Analytical solutions for the non-linear ordinary differential equations (35), (36) and (38), together with boundary conditions (40)–(42) are obtained using Wolfram Mathematica [61], with the material parameters listed in Section 4 and values of the SPE thickness $w = 5$, 10 and 14 μm, as summarized in Table 2 (similarly, a 10 μm thick layer was considered for the SPE in Refs. [33,34]).

Since the mass flux h flowing through the SPE is assigned (boundary conditions (41)) and uniform within the SPE (because of the one-dimensional setting of the mass balance (2)), it follows that the right-hand side of (36) is constant. Negative values of ionic concentration are not physically meaningful and therefore the second term between brackets is always greater than or equal to zero and is directly proportional to the Young's modulus, Poisson's ratio and partial molar volume through the coefficient α (37). The coefficient pre-multiplying the concentration increases if the mechanical contribution is considered and this causes a reduction of the concentration gradients throughout the SPE. To analyze the impact of this coefficient on the results, the upper bound α_{ub} for α is set using $E = 500$ MPa, $\Omega = 1.5 \times 10^{-4}$ m^3 mol^{-1} and a nearly incompressible material defined by means of $\nu = 0.49$. The implication of this specific set of parameters will be discussed shortly.

Fig. 4 shows the concentration and electrostatic potential distribution obtained solving (36) and (38). Figs. 4a–c show that the concentration gradient always reduces when mechanical contributions are included in the model (the slope of the green curves is always steeper than the others). This is in line with the observation of Purkayastha and McMeeking [39] for the contribution of stresses on the lithiation/delithiation of active material particles: “the stress gradient will always aid the process that is being undertaken”. Here, the process is the transfer of ions from the positive (negative) to the negative (positive) electrode during a charging (discharging) process. The results for $E = 5$ MPa are not reported because they are indistinguishable from the electrochemical solution ec obtained with $E = 0$ (green line). The concentration gradient reduction is more pronounced in the set of curves obtained with $\Omega = 1.5 \times 10^{-4}$ m^3 mol^{-1} (continuous lines) compared to those obtained with $\Omega = 1.1 \times 10^{-4}$ m^3 mol^{-1} (dashed lines): a change of roughly 40% has a remarkable impact on the results because the contribution of Ω is quadratic in (36).

For a given value of j_{bc}, the critical width of the SPE is defined as the value of w for which depletion at the negative electrode ($x = 0$) occurs. This value can be determined for the ec case from equation (36) with $\Omega = 0$. The assigned boundary conditions (41) and $j_{bc} = 10$ A m^{-2} lead to a critical width approximately equal to 14.4 μm, explaining why the SPE depletion from ions is almost achieved in Fig. 4c (left edge). For the $w = 14$ μm cell the concentration gradients are the largest and the role of stresses on the concentration gradient reduction is remarkable: up to 50% compared to ec for $E = 500$ MPa with $\Omega = 1.5 \times 10^{-4}$ m^3 mol^{-1} (compare green and orange continuous lines in Fig. 4c), and up to 60% for α_{ub} (compare green and red lines in Fig. 4c).

Once the concentration profile is known, the electrostatic potential and the displacement at any point in the domain can be determined by solving some ordinary differential equations as discussed next. By replacing boundary condition (40b) into (38), the steady state electrostatic potential gradient can be express as

$$\frac{d\phi}{dx} = \frac{1}{\gamma_\phi\, c}\left(\left(\gamma_c + \alpha\,\gamma_p\, c\right)\frac{dc}{dx} + j_{bc}\right), \quad x \in [\,0,\ w\,]. \tag{44}$$

Since each term on the right-hand side is positive (refer to Figs. 4a–c for the concentration gradient) the electrostatic potential gradient is also positive.

Figs. 4d–f show the steady state electrostatic potential corresponding to the ionic concentration distribution of Figs. 4a–c. The ec profiles resemble those determined in previous studies focused on the ionic transport in liquid battery electrolytes [23,24], but the introduction of the mechanical contribution in the model makes them smoother. As a consequence of the non-linearity of (44) this results either in an increase (Fig. 4d) or in a reduction (Fig. 4f) of the overall electrostatic potential difference across the SPE depending on the width w.

For $w = 5$ μm the values assumed by the ionic concentration and its gradient at any location of the SPE width are basically the same for both ec and coupled models, with small variations depending on E, ν, and Ω. Fig. 4a shows that the concentration ranges between 0.65 and 1.35 times c^0 for ec (green line) and between 0.86 and 1.13 times c^0 for α_{ub} (red line). For this geometrical configuration, the term that determines changes in the electrostatic potential profile in (44) is $\alpha\,\gamma_p$. This parameter, linearly proportional to the Young's modulus and quadratically proportional to the partial molar volume, is therefore responsible for the slope increase observed in Fig. 4d for higher E and Ω. For $w = 14$ μm, the concentration c in the denominator of (44) strongly influences the electrostatic potential profile. A steep slope is observed in proximity of the negative electrode ($x = 0$) for the solution that corresponds to the electrochemical model (green line in Fig. 4f), and this pairs with the observation that $c \to 0$ for $x \to 0$ in Fig. 4c. Since the

Table 2
Material parameters, geometrical features, initial and boundary conditions.

Symbol	Quantity	Value
D_{Li^+}	Diffusion constant for Li^+ ions in SPE [32]	2.5×10^{-13} m^2 s^{-1}
$D_{PF_6^-}$	Diffusion constant for PF_6^- ions in SPE [32]	3.0×10^{-13} m^2 s^{-1}
E	SPE Young's modulus [8,9,18,42,43]	5, 50, 140, 500 MPa
ν	SPE Poisson's ratio [9]	0.24
Ω	Combined partial molar volume of $LiPF_6$ in SPE[b]	1.1×10^{-4}, 1.5×10^{-4} m^3 mol^{-1}
$\Omega_{PF_6^-}/\Omega$	Contribution of PF_6^- to the combined partial molar volume[b]	37/38
w	Width of the SPE layer	5, 10, 14 μm
c^0	Salt concentration in SPE [32]	1500 mol m^{-3}
j_{bc}	Charging current [21,32]	10 A m^{-2}
$\bar{k}$	Applied curvature	-5×10^{-3}, 0, 5×10^{-3} μm^{-1}

[b] Refer to Section 4 for details.

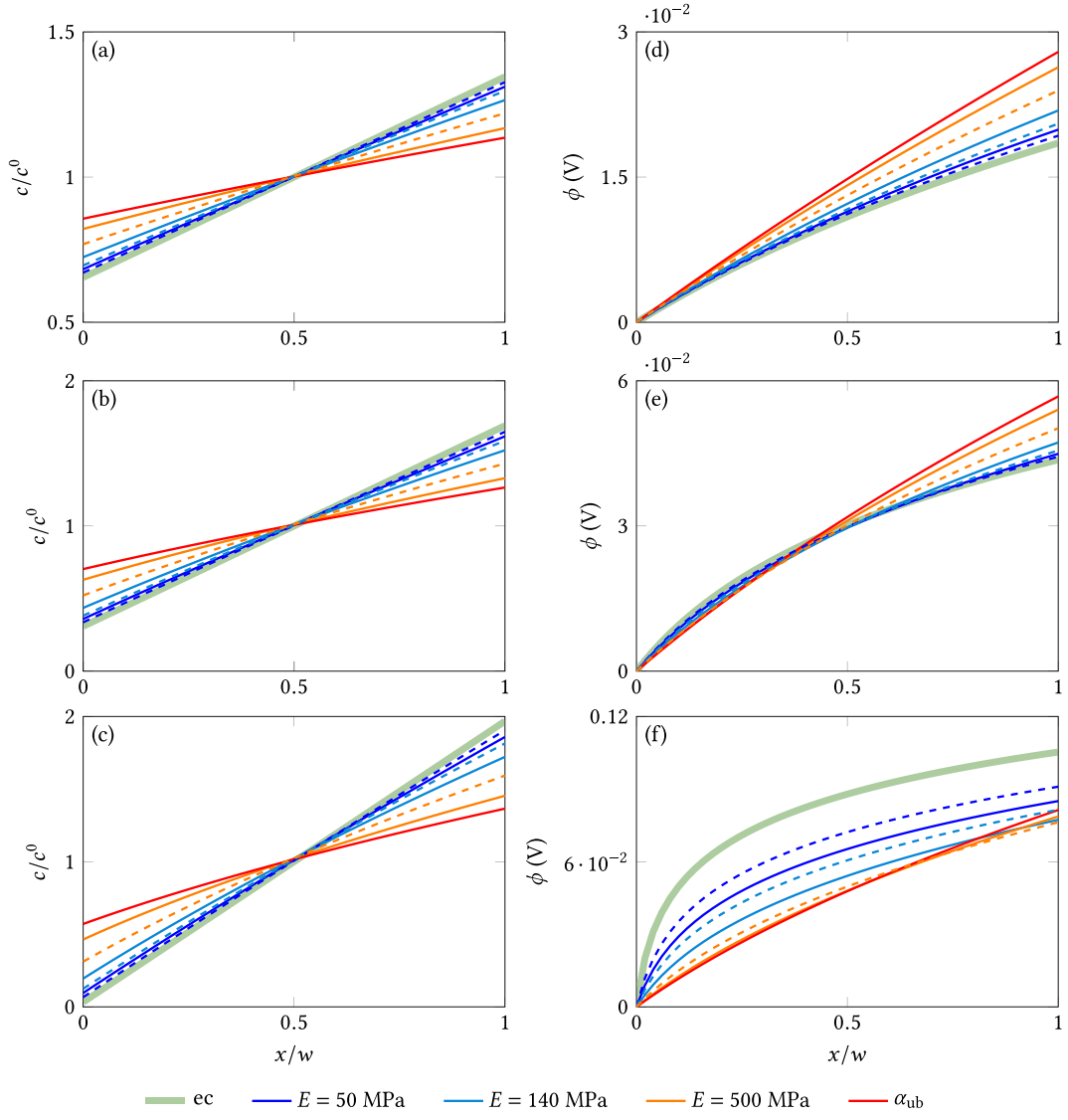

Fig. 4. Steady state profiles of the ionic concentration (a–c) and electrostatic potential (d–f) distributions within the solid polymer electrolyte. Plots refer to three different width of the SPE: (a,d) $w = 5\,\mu$m; (b,e) $w = 10\,\mu$m; (c,f) $w = 14\,\mu$m. The x-coordinate along the width of the SPE is normalized by the width w itself, while the ionic concentration is normalized by the initial concentration $c^0 = 1500$ mol m^{-3}. Continuous lines refer to $\Omega = 1.5 \times 10^{-4}$ m^3 mol^{-1}, dashed lines refer to $\Omega = 1.1 \times 10^{-4}$ m^3 mol^{-1}. Label ec indicates the solution of the electrochemical model.

minimum concentration value at $x = 0$ increases with $\alpha\,\gamma_p$ (about 0.57 c^0 for α_{ub}, instead of 0.03 c^0 for ec), a corresponding reduction of the slope of the electrostatic potential at the same location follows.

The curves ec and α_{ub} represent the upper and lower bounds for the concentration profiles (green and red lines of Figs. 4a–c), as they show the largest and the smallest deviation from c^0, respectively. This observation suggests that given two SPEs with comparable electrochemical properties, the one whose combination of parameters E, ν and Ω allows to maximize α (37) should be favored to limit the risk of ion depletion of the electrolyte during charge/discharge operations. Further details about the impact of stresses on the salt concentration profile are given in Section 6. Nevertheless, Figs. 4d–f suggest that the non-linear nature of (44) requires a specific evaluation to be conducted for each geometry and set of parameters if accurate prediction are needed. The same set of parameters α_{ub} can either lead to a sensible internal resistance increase or reduction compared to the ec solution depending on the geometry (+50% with $w = 5\,\mu$m and −32% with $w = 14\,\mu$m).

From (35), boundary conditions (42) and initial condition (43), the deformation (32) can be expressed as a function of the concentration through

$$\varepsilon = \frac{1+\nu}{1-\nu}\frac{\Omega}{3}\left(c - c^0\right), \quad x \in [0,\ w], \tag{45}$$

and, by integrating both sides, the displacement field is obtained as

$$u(x) = \frac{1+\nu}{1-\nu}\frac{\Omega}{3}\left(\int_0^x c\,(\zeta)\,\mathrm{d}\zeta\ -\ c^0\,x\right), \quad x \in [0,\ w]. \tag{46}$$

Fig. 5 shows that the magnitude of displacement and deformation fields reduces in SPE with higher elastic modulus, in agreement with the results of Purkayastha and McMeeking [39].

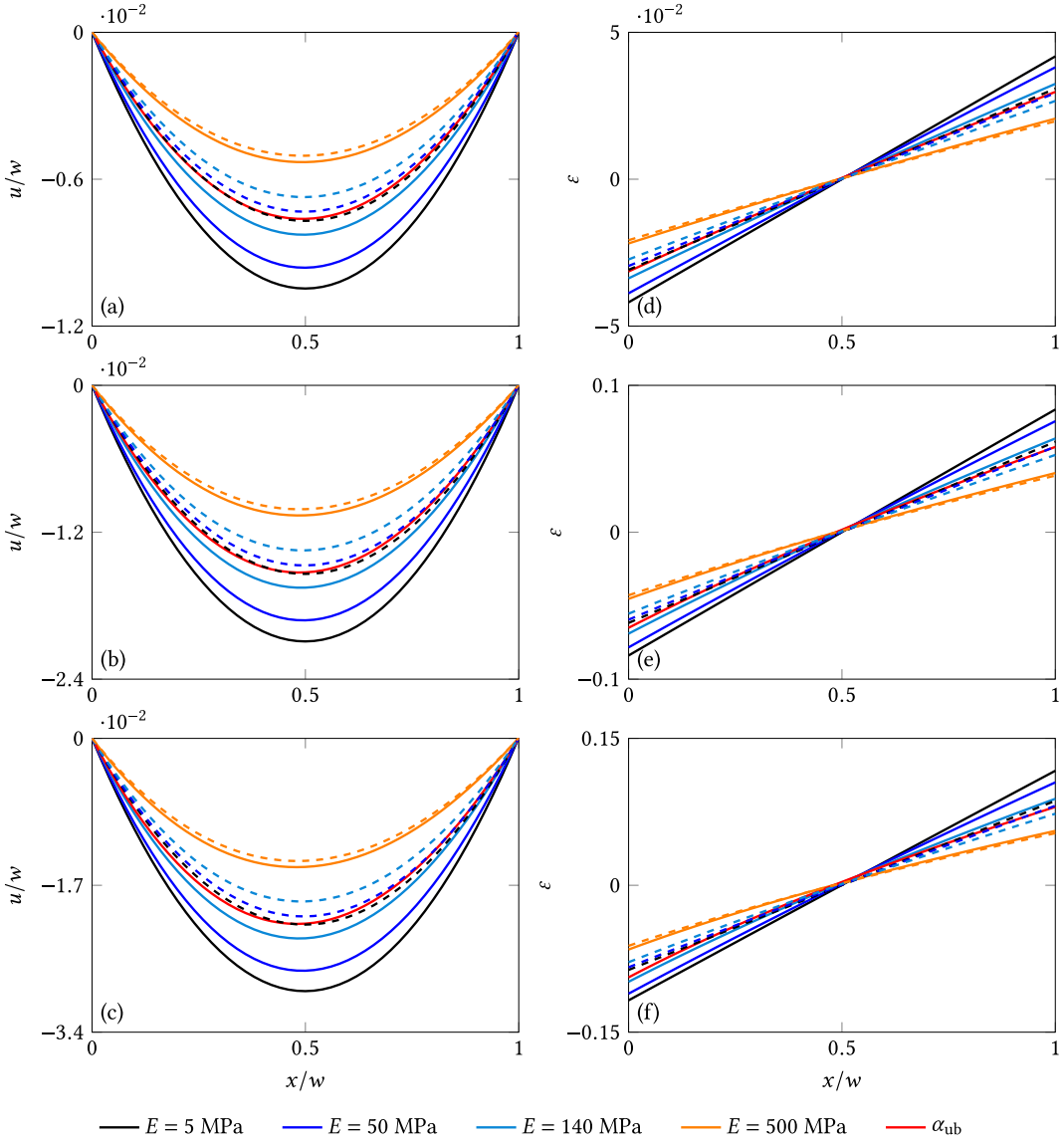

Fig. 5. Steady state profiles of the displacement (a–c) and deformation (d–f) distributions within the solid polymer electrolyte. Plots refer to three different width of the SPE: (a,d) $w = 5\ \mu$m; (b,e) $w = 10\ \mu$m; (c,f) $w = 14\ \mu$m. The x-coordinate along the width of the SPE and the displacement are normalized by the width w itself. Continuous lines refer to $\Omega = 1.5 \times 10^{-4}$ m^3 mol^{-1}, dashed lines refer to $\Omega = 1.1 \times 10^{-4}$ m^3 mol^{-1}.

From (45) and (46) it is evident that both are proportional to $c - c^0$, Ω, and ν. Reduced displacements and deformations are obtained with sets of parameters that limit the extent of the concentration gradients (Fig. 4) while changes in Ω become dominant when concentration distributions are comparable. The results obtained with the set of parameters $E = 500$ MPa, $\Omega = 1.1 \times 10^{-4}$ m^3 mol^{-1} and $\nu = 0.24$ represent the lower bound for both displacements and deformations (dashed orange lines in Fig. 4). Higher displacements and deformations are visible with α_{ub} (red lines) compared to those predicted with the set of parameters $E = 500$ MPa, $\Omega = 1.5 \times 10^{-4}$ m^3 mol^{-1} and $\nu = 0.24$ (continuous orange lines), because the term $(1+\nu)/(1-\nu)$ increases with ν and reaches its maximum value for $\nu = 0.49$ (refer to (45) and (46)). The set of parameters α_{ub} leads neither to a lower nor to an upper bound for any of the mechanical fields in Figs. 5 and 6.

From (34) and (45) the pressure distribution along the SPE is a function of the concentration through

$$p = \frac{2}{9}\frac{E\Omega}{1-\nu}\left(c - c^0\right), \quad x \in [0,\ w]. \tag{47}$$

The components of the stress tensor (33) are

$$\sigma_{xx} = 0, \quad x \in [0,\ w], \tag{48a}$$

$$\sigma_{yy} = \sigma_{zz} = \frac{1}{3}\frac{E\Omega}{1-\nu}\left(c^0 - c\right), \quad x \in [0,\ w]. \tag{48b}$$

Considering the boundary conditions (42) and the initial condition (43), the von Mises stress can be expressed as

$$\sigma_{vM} = \frac{1}{3}\frac{E\Omega}{1-\nu}\left|c^0 - c\right|, \quad x \in [0,\ w]. \tag{49}$$

Fig. 6 shows the pressure (47) and the von Mises stress (49) profiles along the SPE, scaled by the Young's modulus E related to the corresponding parameter set (the same normalization used by

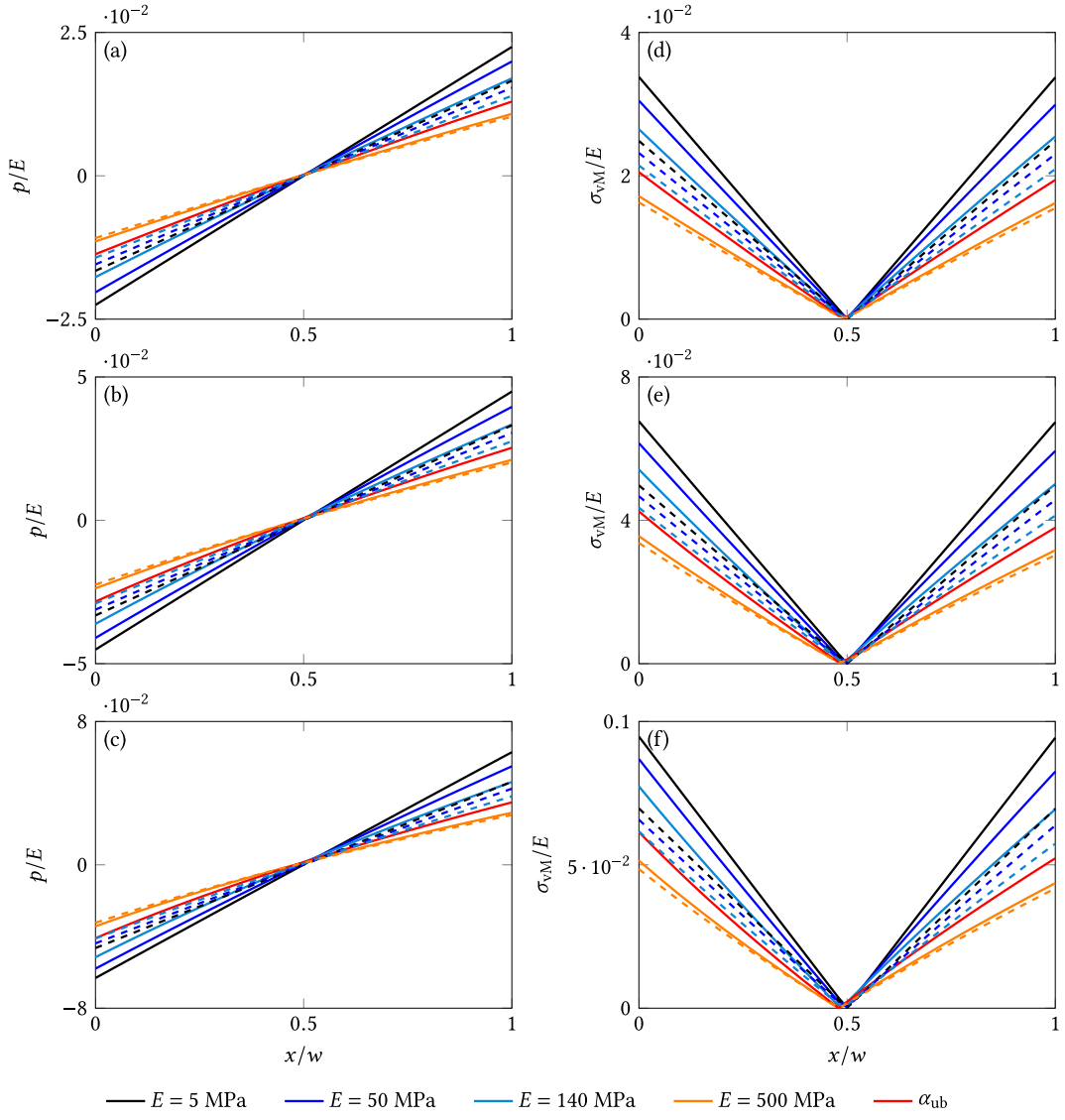

Fig. 6. Steady state profiles of the pressure (a–c) and von Mises stress (d–f) distributions within the solid polymer electrolyte. Plots refer to three different width of the SPE: (a,d) $w = 5\,\mu$m; (b,e) $w = 10\,\mu$m; (c,f) $w = 14\,\mu$m. The x-coordinate along the width of the SPE is normalized by the width w itself, while the pressure and the von Mises stress are normalized by the value of the Young's modulus to which the curve refers. Continuous lines refer to $\Omega = 1.5 \times 10^{-4}$ m^3 mol^{-1}, dashed lines refer to $\Omega = 1.1 \times 10^{-4}$ m^3 mol^{-1}.

Purkayastha and McMeeking [39]). The trend of the pressure matches that of the concentration in Fig. 4. A tensile stress state develops on left side of the SPE where the SPE is depleted from ions, while a compressive stress arise at the opposite boundary where the ions accumulate. Higher values of the pressure p are attained in SPEs characterized by smaller values of the elastic modulus because of the development of more pronounced concentration gradients. The highest values in tension and compression are attained at the boundary of the domain, at the interface with the electrodes. The minimum and maximum values of p are achieved for configuration α_{ub} in the $w = 14\,\mu$m cell and they are equal to -20 and 17.4 MPa corresponding to a tensile stress state at the left edge and a compressive stress state at the right edge. These stress levels are sufficient to impair the structural integrity of the polymer. Amirsadeghi et al. [42] performed experimental tensile tests on PPGDA cross-linked with trimethylolpropane triacrylate (TMPTA) between 0 and 49 weight percent (wt%). The authors report values of Young's modulus that increase from 10 to 215 MPa with increasing TMPTA content, and corresponding values of fracture stress that increase from 0.9 to 10.5 MPa. These values suggest that the fracture stress of PPGDA lies between 5 and 9% of E, depending on the specific composition. According to this rough estimate, Fig. 6 shows that the SPE in the $w = 14\,\mu$m cell may fracture at the electrode-SPE interface, where the absolute value of the pressure p is up to 3–6% E. Since the debonding stress at the electrode-SPE interface depends both on the polymer and the material to which it adheres, its threshold may differ from the fracture stress of the polymer itself and can, in general, be lower [42]. The adhesion between the PEO electrolyte and a vanadium oxide (V_2O_5) film electrode was investigated by Su et al. [20]. In their experimental-numerical study the PEO was modeled as a linear elastic material with Young's modulus equal to 850 MPa, and the mechanical interaction between PEO and V_2O_5 was described through a bilinear cohesive law with maximum strength equal to 85 MPa. A rough estimate can be performed by taking the maximum strength as the upper bound for the debonding stress. A threshold corresponding to 10% of E is identified as a qualitative indicator for failure, in line with the above mentioned values. If the structural integrity of the polymer is

compromised at the electrode-SPE interface, a decreased adhesion is expected and an increased impedance follows [5]. In the worst-case scenario, the polymer detaches from the electrode, thus preventing the charge transfer and leading to battery failure.

Figs. 6d–e show that the von Mises stress σ_{vM} increases linearly from the center of the domain towards the boundaries, where the difference between the steady state concentration and the initial value achieves its maximum. Besides the larger deviation of c from c^0 attained with $\Omega = 1.1 \times 10^{-4}$ m^3 mol^{-1} in Fig. 4, higher values of σ_{vM} correspond to $\Omega = 1.5 \times 10^{-4}$ m^3 mol^{-1} when all the other conditions are fixed. This suggests that the term $(E\,\Omega)/(1-\nu)$ in (49) prevails over $c^0 - c$. The opposite explanation applies when comparing curves α_{ub} against those obtained with $E = 500$ MPa, $\Omega = 1.5 \times 10^{-4}$ m^3 mol^{-1} and $\nu = 0.24$: in spite of a smaller deviations in $c^0 - c$, higher von Mises stress levels are obtained with α_{ub}.

Experimental studies on PEO with Young's modulus in the range 2–50 MPa and 70–325 MPa were performed by Westover et al. [8] and Moreno et al. [18], respectively, and show that either the yield stress [8] or the tensile strength [18] of these materials falls between 3 and 10% of the value of Young's modulus of the polymer. Two conclusions can be drawn. First, since the stress levels lie above the previously mentioned threshold in regions limited to the electrode-SPE interfaces and their surrounding, the use of a linear elastic constitutive behavior would, in average, be a reasonable approximation. In this perspective, a linear elastic constitutive model allows the identification of critical stress level locations and the investigation of the behavior of materials that experimentally show a wide range of mechanical responses [8,9,18,42,43] in a rather simple way (by changing the Young's modulus). Second, if σ_Y lies in the range 3–10% E, Fig. 6 shows that the von Mises stress exceeds this value during routine battery operations, in a situation with no external loads applied to the cell. If the SPE undergoes irreversible deformation or damage, its electrochemical properties may change and the response of the battery can be affected, as showed by Bucci et al. [41,62] in their recent investigation of the correlation between mechanical damage and effective conductivity of all-solid-state battery based on inorganic electrolytes.

Although the use of solid polymer electrolytes for 3-D microbatteries presents several advantages with respect to their liquid counterpart, the low ionic conductivity poses obstacles to their application in high power micro-devices that require the delivery of high electric currents [21]. Experimental studies report further reduction of the ionic conductivity for SPEs characterized by increasingly high values of the stiffness as shown in Fig. 1. Despite these discouraging material-level observations, a different trend holds at the cell level. The steady state conductivity is chosen as the indicator of the electrolyte component and is defined as

$$\overline{\kappa} = \frac{j_{bc}}{\Delta V}, \tag{50}$$

where

$$\Delta V = \phi|_{x=w} - \phi|_{x=0} \tag{51}$$

is the steady state electrostatic potential difference across the width w. The conductivity just introduced coincides with the inverse of the resistivity defined by Zadin et al. [63], but is limited to the electrolyte component. The open circuit voltage of the cell (V_{OC} in Ref. [63]) is considered to be zero because neither the electrodes nor the electrode kinetic was modeled.

Since the electrochemical parameters D_{Li^+} and $D_{PF_6^-}$ were kept unchanged for all the computations, changes in conductivity are merely due to different values of the Young's modulus and partial molar volume (and Poisson's ratio for the α_{ub} case). For each combination of w and Ω, the impact of the elastic modulus on the steady state SPE conductivity is evaluated. Fig. 7 shows the conductivity $\overline{\kappa}$ normalized by the value obtained for the same geometry but using the electrochemical model ($\overline{\kappa}_{ec}$). The plot summarizes the results of six combination of w and Ω and shows the dependence of the conductivity on E. The values of conductivity α_{ub} obtained for each w are provided as well. The plot shows that depending on the polymer width, changes in the mechanical properties of the SPE lead to variations between −30% and +38% in the overall polymer conductivity (50).

The direct proportionality between the conductivity and the elastic modulus for the 14 μm-wide SPE may appear unexpected. Ionic conductivity of SPEs is usually associated with polymer segmental motion, and from a material level perspective it is well-known that a more flexible polymer possesses higher ionic conductivity as schematically shown in Fig. 1. Nevertheless, the results just reported call for a different interpretation. The focus of this study is on the investigation of the (electrochemical) response of polymer electrolytes showing similar electrochemical behavior (comparable values of ionic conductivity and ionic diffusivity) but different mechanical properties (due, e.g., to different composition or presence of additives [15–19]). The reduction of the SPE's resistivity (50) follows from the contribution of the pressure gradient (20) to the ionic conduction. The electric current that flows through the SPE induces a redistribution of ions and the development of a concentration gradient. The mechanical stresses that arise in response to this process oppose to the accumulation of ions in some regions (inducing a pressure stress state) and the depletion (inducing tension stress state) of others, thus promoting the flow of ions in the same direction of the electric current. This chain of events makes the overall SPE system (not the material) less resistive. Finally, no external mechanical loads were applied to the system: the stresses are related to the redistribution of ions throughout the SPE. The results just presented should not be misunderstood. In general, an improvement of mechanical properties does not compensate the material level conductivity reduction that pairs with it; nevertheless, we stress that the

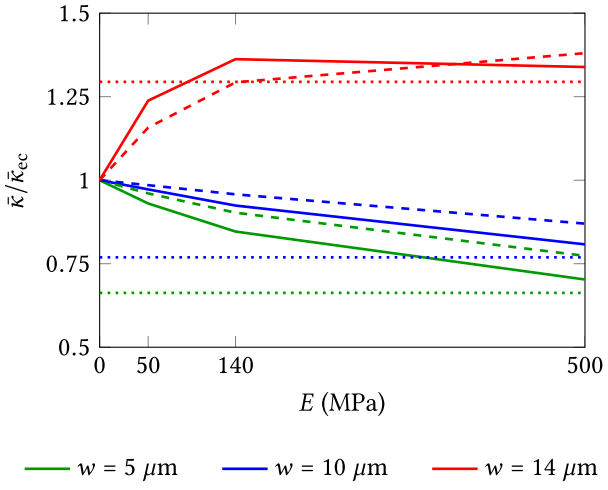

Fig. 7. The system conductivity changes within the SPE for different values of its Young's modulus. The results refer to the solid polymer electrolyte layers of different width w. Continuous lines refer to $\Omega = 1.5 \times 10^{-4}$ m^3 mol^{-1}, dashed lines refer to $\Omega = 1.1 \times 10^{-4}$ m^3 mol^{-1}, and dotted lines refer to the combination of values α_{ub} (the same color is used to identify a w value). (For interpretation of the references to color in this figure legend, the reader is referred to the Web version of this article.)

electrochemical-mechanical interaction can be exploited to mitigate this trend. With reference to the ideal relationship in Fig. 1, this is of special interest for materials that fall in the bottom right portion of the graph. For those materials, large improvements in mechanical properties lead to negligible reductions of their electrochemical properties, and this is clearly supported by experimental evidence [45].

These considerations apply to both values used for the partial molar volume: over the wide range of Young's modulus values explored in this study, modest effects on the results are observed for variation of the partial molar volume of about 25%.

6. Uniform planar cell: externally induced deformations

The concentration gradient that develops across the SPE is one of the limiting factor for its utilization. If the limit of zero concentration is achieved at the electrode-SPE interface, no further SPE-electrode lithium transfer occurs and the charge/discharge process stops. In this section we show how externally applied mechanical loads can potentially be exploited to reduce the concentration profile in the SPE.

We are interested in conditions similar to those of a uniform planar cell. We assume that the extension of the cell in the z-direction is such that charge and mass fluxes have no z-component and that plane strain conditions are suitable for the mechanical description. The width of the film in Fig. 8 is w and its height is $H = 2h$. A galvanostatic process is considered and the negative electrode is selected as the reference electrode therefore implying

$$\phi(t)|_{x=w} = 0, \quad y\in[-h,h],\ t\in[0,t_{\text{end}}) \text{ and} \tag{52a}$$

$$\boldsymbol{j}(t)\cdot\boldsymbol{n}|_{x=w} = -j_{bc}, \quad y\in[-h,h],\ t\in[0,t_{\text{end}}). \tag{52b}$$

The boundary conditions

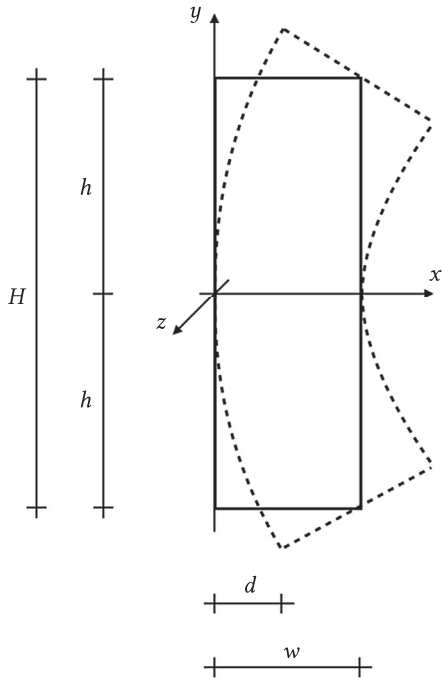

Fig. 8. Schematic of SPE layer cross section with ($\bar{k}>0$; dashed line) and without ($\bar{k}=0$, solid line) bending.

$$\boldsymbol{h}\cdot\boldsymbol{n}|_{x=w} = -\boldsymbol{h}\cdot\boldsymbol{n}|_{x=0} = -\frac{1}{F}\frac{D_{\text{PF}^-}}{D_{Li^+}+D_{\text{PF}^-}}j_{bc}, \quad y\in[-h,h],\ t\in[0,t_{\text{end}}) \tag{53}$$

apply to the mass conservation equation according to (25). Homogeneous boundary conditions are applied on top and bottom edges:

$$\boldsymbol{j}\cdot\boldsymbol{n}|_{y=-h} = \boldsymbol{j}\cdot\boldsymbol{n}|_{y=h} = 0, \quad x\in[0,w],\ t\in[0,t_{\text{end}}) \text{ and} \tag{54a}$$

$$\boldsymbol{h}\cdot\boldsymbol{n}|_{y=-h} = \boldsymbol{h}\cdot\boldsymbol{n}|_{y=h} = 0, \quad x\in[0,w],\ t\in[0,t_{\text{end}}). \tag{54b}$$

To obtain a pressure gradient along the x-direction, a uniform curvature is induced in the SPE by applying the boundary conditions [64].

$$u_y^{\text{bc}} = -\bar{k}\left(x-\frac{w}{2}\right)y, \quad y=h, \quad y=-h, \quad x\in[0,w], \quad t\in[0,t_{\text{end}}) \tag{55}$$

at the bottom ($y = -h$) and top ($y = h$) boundaries, with $\bar{k}$ the parameter that defines the curvature. We assume that the deformation of the electrodes is compliant with that of the SPE and that a traction-free regime exists along the electrode-SPE interfaces at $x = 0$ and $x = w$:

$$\boldsymbol{\sigma}\,\boldsymbol{n}\,|_{x=0} = \boldsymbol{\sigma}\,\boldsymbol{n}\,|_{x=w} = 0\,, \qquad y\in[-h,h],\ t\in[0,t_{\text{end}}). \tag{56}$$

This assumption is made to simplify the derivations such that a procedure similar to that adopted in Section 5 can be followed. Thanks to this simplification we show that the extent of the salt concentration gradient can be adjusted by just tuning a single parameter (the curvature $\bar{k}$). The problem is reduced to a single one-dimensional differential equation for which an analytical solution is identified (at least for some set of parameters, as discussed later). Moreover, the focus of this section is to highlight how electrochemical-mechanical coupling affects the concentration gradient rather than providing a thorough description of a real situation. According to (55) the vertical displacement u_y^{bc} varies linearly along the x coordinate and is zero along the middle axis ($x = w/2$). Fig. 8 shows that for $\bar{k}>0$ tension and compression stress states in the regions $x\in[0,w/2)$ and $x\in(w/2,w]$ are induced, respectively. Finally, the SPE is assumed to perfectly adhere to the electrodes during the whole process. The electric current density j_{bc} is kept constant accordingly.

6.1. Results and discussion

Similar to Section 5.1, we focus on the steady state because it is the configuration at which the largest deviation from the uniform concentration distribution is attained. At the steady state the displacement field components take the form

$$u_x = \bar{u}(x) + \frac{1}{2}\bar{k}\,y^2, \quad u_y = -\bar{k}\left(x-\frac{w}{2}\right)y, \quad u_z = 0, \quad x\in[0,w],\ y\in[-h,h]. \tag{57}$$

The displacement component u_x has been decomposed into contributions $\bar{u}(x)$ and $1/2\,\bar{k}\,y^2$ that depend on the x and y coordinate, respectively. Next, we prove that the relations in (57) satisfy equilibrium equation and boundary conditions. Substitution of the strain tensor (6) components corresponding to the displacement field in (57),

$$\varepsilon_{xx} = \frac{\partial \overline{u}}{\partial x}, \quad \varepsilon_{yy} = -\overline{k}\left(x - \frac{w}{2}\right), \quad \varepsilon_{zz} = \varepsilon_{xy} = \varepsilon_{xz} = \varepsilon_{yz} = 0, \quad x \in [0,\ w],\ y \in [-h, h], \tag{58}$$

into equilibrium equation (22c) yields

$$\frac{\partial^2 \overline{u}}{\partial x^2} = \frac{\nu}{1-\nu}\overline{k} + \frac{1+\nu}{1-\nu}\frac{\Omega}{3}\frac{\partial c}{\partial x}, \quad x \in [0,\ w],\ y \in [-h, h] \text{ and} \tag{59a}$$

$$\frac{\partial c}{\partial y} = 0, \quad x \in [0,\ w],\ y \in [-h,\ h]. \tag{59b}$$

These equations allow to identify a relationship analogous to (35) between displacements and concentration along the x-coordinate and to state that no salt concentration gradient develops in the y-coordinate. With reference to (58), the pressure field (20) is expressed as

$$p = K\left(\Omega\left(c - c^0\right) + \overline{k}\left(x - \frac{w}{2}\right) - \frac{\partial \overline{u}}{\partial x}\right), \quad x \in [0,\ w],\ y \in [-h,\ h]. \tag{60}$$

Its combination with (59a) allows to rephrase the apparent mass flux (18) components as

$$h_x = -\left(D + \alpha\frac{1}{2}\frac{D}{RT}\,\Omega\, c\right)\frac{\partial c}{\partial x} - \alpha\frac{3}{4}\frac{D}{RT}\, c\,\overline{k}, \quad x \in [0,\ w],\ y \in [-h,\ h] \text{ and} \tag{61a}$$

$$h_y = -\left(D + \alpha\frac{3}{4}\frac{D}{RT}\,\Omega\,\frac{1-\nu}{1-2\nu}c\right)\frac{\partial c}{\partial y}, \quad x \in [0,\ w],\ y \in [-h,\ h]. \tag{61b}$$

The mass flux component h_x equals (36) with the addition of the term proportional to $\overline{k}$, while it follows from (59b) that h_y is identically equal to zero, making boundary conditions (54b) trivially satisfied. Since the mass flux is one-dimensional, the value of h_x at any point of the domain equals the boundary condition applied along the vertical boundaries. Substitution of (53) into (61) yields the one-dimensional non-linear differential equation in c

$$\left(D + \alpha\frac{1}{2}\frac{D}{RT}\,\Omega\, c\right)\frac{\mathrm{d}c}{\mathrm{d}x} = \frac{1}{F}\frac{D_{PF^-}}{D_{Li^+} + D_{PF^-}} j_{bc} - \alpha\frac{3}{4}\frac{D}{RT}\, c\,\overline{k}, \quad x \in [0,\ w], \tag{62}$$

that must be solved in combination with the constraint

$$\frac{1}{w}\int_0^w c(\zeta)\,\mathrm{d}\zeta = c^0. \tag{63}$$

This requirement states that the overall amount of salt in the SPE must be preserved (we take $c^0 = 1500\ \mathrm{mol\ m^{-3}}$, as before). Equation (62) shows that it is possible to determine a value of $\overline{k}$ such that the desired mass flux flows in absence of concentration gradient. Since the term between brackets in (62) is strictly positive, the left-hand side of (62) vanishes if and only if $\mathrm{d}c/\mathrm{d}x = 0$. If condition $\mathrm{d}c/\mathrm{d}x = 0$ holds, the concentration distribution is uniform and equal to c^0 according to (63). The right-hand side of (62) can therefore be set equal to zero to determine the value of $\overline{k}$ at which a mass flux flows with no concentration gradient yielding

$$\overline{k} = 3\,\frac{RT}{F}\,\frac{1-\nu}{E}\,\frac{1}{\Omega\, c^0}\,\frac{1}{D_{Li^+}}\, j_{bc}. \tag{64}$$

This expression clearly shows that the curvature required to achieve condition $\mathrm{d}c/\mathrm{d}x = 0$ is higher for higher applied current j_{bc} while it is lower for higher Li-ions diffusivity D_{Li^+}, partial molar volume Ω and Young's modulus E values.

Irrespective of the value of $\overline{k}$, once the salt concentration distribution c is know, integration of (59) together with boundary conditions (56) allows to determine $\overline{u}$. Its expression reads

$$\overline{u} = \frac{\nu}{1-\nu}\overline{k}\,(x - w)\frac{x}{2} + \frac{1+\nu}{1-\nu}\frac{\Omega}{3}\left(\int_0^x c(\zeta)\,\mathrm{d}\zeta - c^0\, x\right), \quad x \in [0,\ w], \tag{65}$$

for a displacement field such that $u_x = 0$ for $x = 0,\ y = 0$. This condition is enforced to avoid rigid body translations. The concentration distribution that satisfies (62) and (63) together with the displacement field defined by (57) and (65) satisfies also the mass balance equation (22b) at the steady state, the equilibrium equation (22c), and boundary conditions (53), (55) and (56). These relations are thus the solution that we are looking for.

Substitution of (65) into (60) leads to an expression for the pressure as a function of the salt concentration

$$p = \frac{E}{3(1-\nu)}\left(\frac{2}{3}\,\Omega\left(c - c^0\right) + \overline{k}\left(x - \frac{w}{2}\right)\right), \quad x \in [0,\ w]. \tag{66}$$

As for (62) this expression is analogous to that determined in Section 5.1, apart for the term that depends on the curvature. Since concentration and pressure gradients vanish along the y-coordinate, boundary conditions (54) make the electric current density one-dimensional as well. Substitution of (66) into definition (13) together with boundary condition (52) leads to

$$\frac{\mathrm{d}\phi}{\mathrm{d}x} = \frac{1}{\gamma_\phi\, c}\left(\left(\gamma_c + \alpha\,\gamma_p\, c\right)\frac{\mathrm{d}c}{\mathrm{d}x} + j_{bc} + \frac{3}{2}\frac{\overline{k}}{\Omega}\alpha\,\gamma_p\, c\right), \quad x \in [0,\ w]. \tag{67}$$

This partial differential equation is used to determine the electric potential profile along the x-coordinate.

The results reported in this section refer to $\Omega = 1.5 \times 10^{-4}\ \mathrm{m^3\ mol^{-1}}$, $w = 10\ \mu\mathrm{m}$ and $E = 140$ and 500 MPa. Furthermore, two boundary conditions for the electric current density ($j_{bc} = 0$ and $10\ \mathrm{A\ m^{-2}}$) and three different curvature values ($\overline{k} = 5 \times 10^{-3}$, 0, and $-5 \times 10^{-3}\ \mu\mathrm{m^{-1}}$) have been considered. The second curvature value refers to an undeformed configuration, while the first and the third correspond to deformed configurations that favorably (i.e., reduce) and unfavorably (i.e., increase) affect the concentration gradient during the charging process. A pressure gradient with opposite slope develops in these two cases. The effect of positive and negative $\overline{k}$ on the concentration gradient reverses during discharge processes. It should be remarked that since boundary conditions (42) are compatible with a stress-free solution (33), in the same way a stress-free boundary condition (56) leads to a homogeneous displacement solution at $x = 0$ and $x = w$, and the solutions for all the other variables are identical to those reported in Section 5.

Analytical solutions for (62) are determined with Wolfram Mathematica [61] in all cases exception made for the combination of boundary conditions $j_{bc} = 10\ \mathrm{A\ m^{-2}}$ and $\overline{k} = -5 \times 10^{-3}\ \mu\mathrm{m^{-1}}$. In this case Mathematica cannot find an analytical solution that

satisfies (62) and constraint (63) at the same time. For the above mentioned combination of boundary condition the problem is solved using our own finite element implementation for the problem, detailed in a companion paper [11]. As a sanity check, finite element simulations are performed for all the combinations of boundary conditions and the results are in perfect agreement with the analytical cases.

Fig. 9 shows the steady state concentration and pressure profiles along the x-axis when $\bar{k} = 5 \times 10^{-3}$ μm^{-1} and no electric current is flowing (opposite sign of $\bar{k}$ would cause the plots to be flipped from right to left). When the SPE is under bending, the equilibrium configuration ($j_{bc} = 0$) does not correspond to a uniform concentration distribution. In contrast with the situation observed during a charging process considered in Section 5, Fig. 4, a concentration gradient with a negative slope develops. This gives a hint on how externally applied mechanical loads influence the concentration distribution across the SPE. In Fig. 9b the pressure profile corresponding to a purely mechanical solution (no electrochemical-mechanical coupling) for the SPE under bending is reported (the pressure profiles for $E = 140$ and $E = 500$ MPa coincide when scaled by the respective Young's modulus). The absolute value of the pressure reduces when the coupling is considered in agreement with definition (7). The term $K\,\Omega\,(c - c^0)$ is indeed positive for $x \in [0, w/2)$ where the SPE undergos traction (negative p) and is negative for $x \in (w/2, w]$ where the SPE undergoes compression (positive p). As expected, the impact of the bending on the concentration distribution is more pronounced for $E = 500$ MPa (Fig. 9a).

Fig. 10 shows the steady state concentration and pressure profiles along the x-axis when the SPE is under bending while the charging process is ongoing. For each value of E the results corresponding to $\bar{k} = 5 \times 10^{-3}$, 0 and -5×10^{-3} μm^{-1} are reported. When $E = 500$ MPa a reduction of the concentration gradient of about 14% is observed with the favorable curvature ($\bar{k} > 0$), while an increase of about 6% corresponds to the unfavorable curvature ($\bar{k} < 0$). These figures reduce to 9% in gradient reduction and 5% in gradient increase with $E = 140$ MPa. Ideally, the concentration gradient could be further reduced with a more pronounced deformation regime. According to (64) the curvatures needed to set the concentration gradient to zero are approximately equal to 2×10^{-2} and 7×10^{-2} μm^{-1} for $E = 500$ and 140 MPa, respectively. The reason why smaller curvature values have been used in the

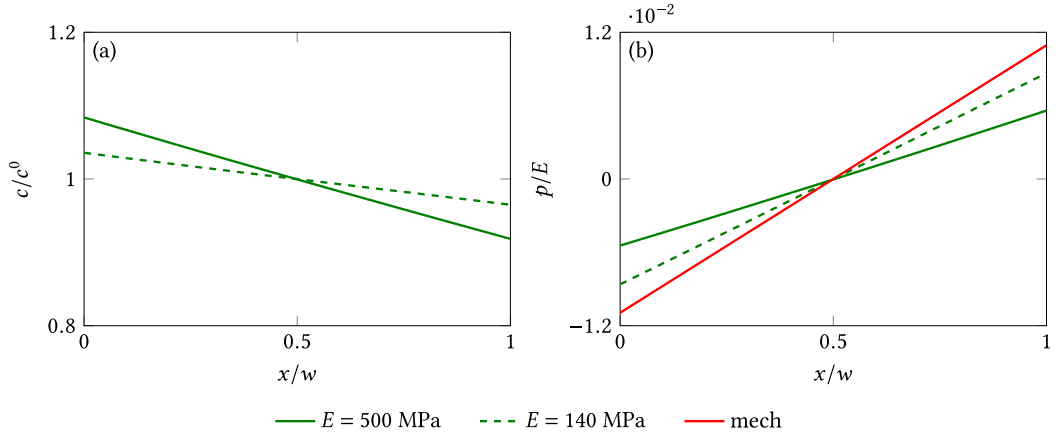

Fig. 9. Steady state profiles of the ionic concentration (a) and pressure (b) distributions within the solid polymer electrolyte. The x-coordinate along the width of the SPE is normalized by the width w itself, while the ionic concentration and the pressure are normalized by the initial concentration $c^0 = 1500$ mol m^{-3} and the Young's modulus, respectively. The results refer to $j_{bc} = 0$ and $\bar{k} = 5\times^{-3}$ μm^{-1} (green curves). Label mech indicates the solution of the mechanical model without coupling (red curve). (For interpretation of the references to color in this figure legend, the reader is referred to the Web version of this article.)

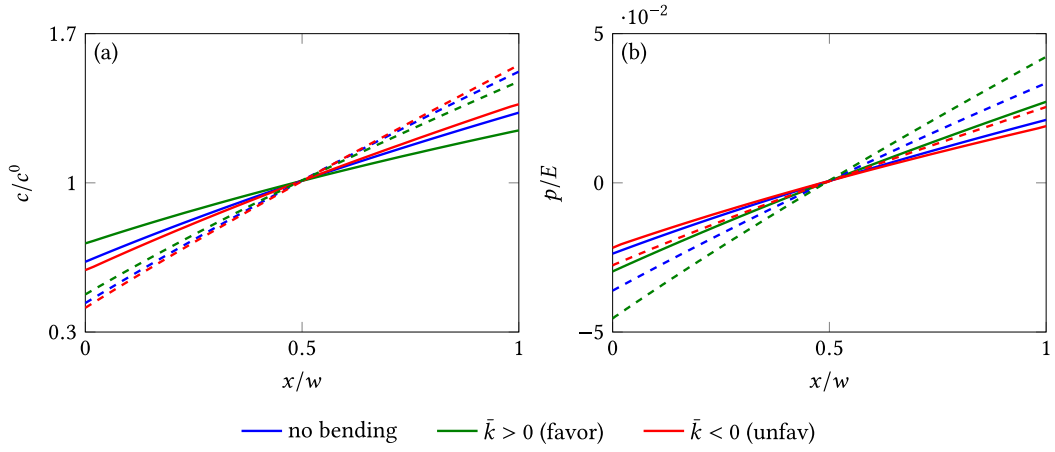

Fig. 10. Steady state profiles of the ionic concentration (a) and pressure (b) distributions within the solid polymer electrolyte. The x-coordinate along the width of the SPE is normalized by the width w itself, while the ionic concentration and the pressure are normalized by the initial concentration $c^0 = 1500$ mol m^{-3} and the Young's modulus, respectively. Continuous lines refer to $E = 500$ MPa, dashed lines refer to $E = 140$ MPa.

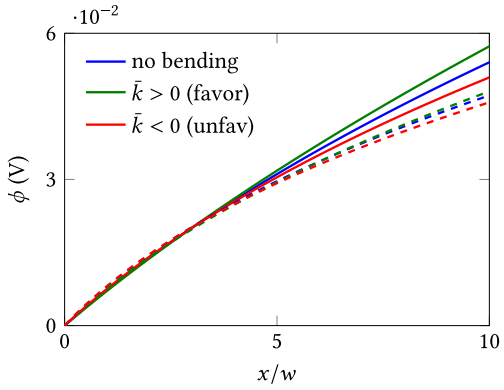

Fig. 11. Steady state profiles of the electric potential distribution within the solid polymer electrolyte. The x-coordinate along the width of the SPE is normalized by the width w itself. Continuous lines refer to $E = 500$ MPa, dashed lines refer to $E = 140$ MPa.

examples is twofold. First, von Mises stresses have been evaluated to be up to 6% and 4% E for the favorable and unfavorable bending, respectively, and thus the limit for linear elasticity analysis to hold is already approached using $\bar{k} = 5 \times 10^{-3}$ μm^{-1}. Second, even if the deformations in the SPE remain small, up to 7% at most, the deflection d (Fig. 8) required to attain the desired curvature becomes remarkable when h/w ratios are large, because the deflection is proportional to h^2. A curvature $\bar{k} = 0.005$ μm^{-1} corresponds to a maximum deflection equal to 1.5 μm for a slab with $h = 25$ μm ($H = 50$ μm), while the deflection is up to approximately 6 μm for $h = 50$ μm ($H = 100$ μm), i.e., more than half of the SPE width.

Fig. 11 shows that the effect of bending on the electric potential drop across the SPE is different compared its effect on the concentration. When the bending is such that it causes a reduction in the concentration gradient ($\bar{k} > 0$ favorable) it also causes a larger potential drop in the SPE. In other words the effective conductivity of the SPE decreases. The effect is reversed when $\bar{k} < 0$.

7. Conclusions

A coupled electrochemical-mechanical model for solid polymer electrolytes has been presented and applied to study the effect of the coupling on the performance of the battery electrolyte. The prediction of the SPE conductivity changes considerably when mechanical contribution is included in the analyses, suggesting that stresses and deformations should be properly accounted for in battery design [63]. This aspect is extremely important for structural batteries as they are expected to experience additional stresses arising from the mechanical loads they bear during service.

The width of the electrolyte determines if the stresses have a detrimental or beneficial impact on performance. The conditions experienced by a solid polymer electrolyte placed in a battery are expected to emphasize the favorable effect of higher Young's modulus compared to those experienced by the same polymer during an impedance spectroscopy test, the experimental technique by which the ionic conductivity of SPEs is usually assessed [4,8,9,15,17,19]. Impedance spectroscopy is performed by applying an alternate electric signal to the SPE, from which the ionic conductivity is indirectly determined. The application of a time-varying electrical load limits the formation of ionic concentration gradients and thus the development of a stress field during the test. For this reason, the mechanical contribution is expected to play a modest role in this kind of experiments.

Apart from the direct influence of mechanical fields on the electrochemical performance of polymer electrolytes, other indirect consequences can be envisaged as the stress level predicted in the SPE is considerable. Figs. 5 and 6 show that mechanical solicitations in the SPE are more pronounced at the interface with the electrodes than elsewhere. The attained stress levels can potentially lead to SPE degradation at the interface and/or reduce the electrode-SPE adhesion [20], causing an increased interface impedance [5]. The stress field at the electrode-electrolyte interface is also determinant for the onset and evolution of dendrite growth [13], which is known as one of the most relevant parasitic processes that can occur in batteries. The deformations induced in the electrodes by the lithium insertion/extraction processes are not considered in this contribution. It is however expected that the inclusion of these process in the model would result in even more severe stress conditions at the interface. During a charge process, lithium is extracted from the positive electrode and inserted into the negative electrode, causing the contraction (for most active materials with a few exceptions [65]) of the former and the expansion of the latter. Figs. 5d–f however show that the SPE contracts and expands in the negative and positive electrodes, respectively. This means that the electrode and electrolyte in contact at the interface undergo opposite deformation states, and this can either result in a stress concentration or in the detachment of the SPE from the electrode. The loss of integrity at the SPE-electrode interface would unavoidably lead to reduced performance and eventually to battery failure.

Externally induced deformations alter the electrochemical response of the film impacting on the salt concentration gradient. Fig. 10 shows that the stress field that develops in the polymer can either increase or reduce the range of application of the SPE film in terms of the electric current. Stresses can indeed either reduce or favor the salt concentration depletion at the SPE-electrode interface. This conclusion, which cannot be drawn from a purely electrochemical evaluation, can have a large impact on the design of flexible microbatteries as they supposed to experience considerable deformation levels and sustain load during service [66].

When 3-D battery architectures are considered, the governing equations are not amenable to analytical solutions and numerical simulations need to be performed. This is the focus of a companion paper [11].

Conflicts of interest

There are no conflicts to declare.

Acknowledgements

The research leading to these results has received funding from the European Research Council under the European Union's Seventh Framework Programme (FP7/2007-2013)/ERC Grant agreement n° 617972.

Appendix A. Maxwell stress contribution

A rough estimate of the Maxwell stress is provided based on the results presented in Section 5. The aim of these derivations is to show that the Maxwell stress can be neglected in the context of this study.

The Maxwell stress tensor for electrostatic fields can be defined as [13]

$$\boldsymbol{\tau} = \varepsilon_0\, \varepsilon_r \left(\nabla\phi \otimes \nabla\phi - \frac{1}{2}(\nabla\phi\cdot\nabla\phi)\mathbf{1} \right) \tag{A.1}$$

where $\varepsilon_0 = 8.854 \times 10^{-12}$ F m^{-1} and ε_r are the vacuum and relative permittivity, respectively. Because of the one-dimensional formulation presented in Section 5, the components of $\boldsymbol{\tau}$ reduce to $\tau_{11} = \tau$ and $\tau_{22} = \tau_{33} = -\tau$, where

$$\tau = \frac{1}{2}\varepsilon_0\, \varepsilon_r \left(\frac{\partial\phi}{\partial x}\right)^2$$

while all the other components are zero.

The contributions of the Maxwell stress to the pressure (in modulus) and to the von Mises stress (49) are evaluated as

$$p^\tau = \frac{|\mathrm{tr}\,\boldsymbol{\tau}|}{3} = \frac{\tau}{3}, \quad \sigma^\tau_{\mathrm{vM}} = 2\tau,$$

respectively. These quantities are compared against the results of the simulations reported in Fig. 6. According to definition (A.1) the Maxwell stress is quadratically proportional to the electrostatic potential gradient, while it is independent of the mechanical properties of the SPE. Based on the results summarized in Fig. 4 and making use of the approximation

$$\frac{\partial\phi}{\partial x} \approx \frac{\Delta V}{w} \tag{A.2}$$

the Maxwell stress is maximized for $\Delta V \approx 0.105\ V$ and $w = 14\ \mu$m, leading to $\Delta V/w \approx 7.5 \times 10^3$ V m^{-1}. Moreover, since the stresses induced by the ionic redistribution within the SPE are proportional to the elastic modulus, if the contribution of the Maxwell stress is negligible for the smallest value of E considered, it is therefore negligible also in all the other cases.

Referring to the $w = 14\,\mu$m cell and taking $E = 5$ MPa, the maximum values obtained for the pressure (in modulus) and for the von Mises stress as shown in Fig. 6 are

$$\frac{p}{E} = 6.32 \times 10^{-2}, \quad \frac{\sigma_{\mathrm{vM}}}{E} = 9.47 \times 10^{-2},$$

and by normalizing p^τ and $\sigma^\tau_{\mathrm{vM}}$ by the same value of E one has

$$\frac{p^\tau}{E} \approx \frac{1}{6}\frac{\varepsilon_0\, \varepsilon_r}{E}\left(\frac{\Delta V}{w}\right)^2 \approx 2\varepsilon_r \times 10^{-11},$$
$$\frac{\sigma^\tau_{\mathrm{vM}}}{E} \approx \frac{\varepsilon_0\, \varepsilon_r}{E}\left(\frac{\Delta V}{w}\right)^2 \approx \varepsilon_r \times 10^{-10}.$$

This means that the contribution of the Maxwell stress becomes significant (p^τ and $\sigma^\tau_{\mathrm{vM}}$ amount to at least 5% of p and σ_{vM}) if the relative permittivity of the SPE is $\varepsilon_r \geq 10^7$, which is taken as the threshold of interest.

To the best of the authors' knowledge, there is no experimental consensus on the value of ε_r for solid polymer electrolytes. However, even if a wide range of values is reported for the relative permittivity of PEO—from 5 to 2000 [67–71] depending on molecular weight, composition, presence of dissolved salt and additives—all the experimental values lie below the previously mentioned threshold.

The Maxwell stress is expected to be more relevant in regions where the electrostatic potential gradient strongly deviates from approximation (A.2) (for example when approaching $x = 0$ for the $w = 14\,\mu$m cell, Fig. 4f), nevertheless it is reasonable to neglect its contribution. Similar arguments led Natsiavas et al. [13] to neglect the Maxwell stress in the modeling of LiPON.

Appendix B. Simulation settings for MD equilibration of PEO

To account for charge polarization effects, the simulations of pure and $LiPF_6$-doped PEO were performed using the MD package LAMMPS [72] with the reactive empirical force field ReaxFF [73], combined with charge equilibration according to [74], in the implementation of Aktulga et al. [75]. A force field parameter set that describes C/H/P/F/O/S/Li interactions, previously applied to energy storage related systems [44,76,77], was used. The simulated PEO structure consists of three linear chain polymers of molecular weight $M = 10062.10$ g mol^{-1} and $LiPF_6$ molecules at a concentration of Li:O = 1:20 yielding a system of 5069 atoms with an average cell dimension of 38 Å. For the equilibration simulations under constant temperature and pressure ensemble (NPT) conditions at 1 atm and 300 K, Verlet time integration with an integration step of 0.25 fs and Nose-Hoover-type baro- and thermostat with pressure and temperature damping constants of 25 fs and 250 fs, respectively, were employed. The lengths of the equilibration simulations were approximately 500 ps and 400 ps for the pure and salt-doped PEO structures, respectively. The initial structures for equilibration were obtained from low density structures of randomly placed molecules using NPT ensemble at 600 K and 10000 atm with Langevin thermostat (damping constant 25 fs) and Nose-Hoover-type barostat (damping constant 250 fs).

Due to the rubbery (i.e., close to glass transition) material state and the comparatively large computational expense of reactive MD simulations, an estimate of dispersion of mass density employing topologically or configurationally diverse SPE cells was not performed. We point out, however, that, according to an earlier MD-based study [78], the microscopic polymer stress-strain response of generic polymer melts has been found to be insensitive to heterogeneities due to crosslinking.

References

[1] K. Murata, S. Izuchi, Y. Yoshihisa, An overview of the research and development of solid polymer electrolyte batteries, Electrochim. Acta 45 (8) (2000) 1501–1508.
[2] K. Edström, D. Brandell, T. Gustafsson, L. Nyholm, Electrodeposition as a tool for 3D microbattery fabrication, Electrochem. Soc. Interface 20 (2) (2011) 41–46.
[3] D. Hallinan Jr., N. Balsara, Polymer electrolytes, Annu. Rev. Mater. Res. 43 (1) (2013) 503–525.
[4] L. Asp, E. Greenhalgh, Structural power composites, Compos. Sci. Technol. 101 (2014) 41–61.
[5] X. Su, K. Guo, T. Ma, P. Tamirisa, H. Ye, H. Gao, B. Sheldon, Deformation and chemomechanical degradation at solid electrolyte-electrode interfaces, ACS Energy Lett. 2 (8) (2017) 1729–1733.
[6] D. Golodnitsky, E. Peled, Stretching-induced conductivity enhancement of LiI–(PEO)-polymer electrolyte, Electrochim. Acta 45 (8) (2000) 1431–1436.
[7] D. Golodnitsky, E. Livshits, Y. Rosenberg, E. Peled, S.H. Chung, Y. Wang, S. Bajue, S.G. Greenbaum, A new approach to the understanding of ion transport in semicrystalline polymer electrolytes, J. Electroanal. Chem. 491 (1) (2000) 203–210.
[8] A. Westover, F. Shabab, J. Tian, S. Bernath, L. Oakes, W. Erwin, R. Carter, R. Bardhan, C. Pint, Stretching ion conducting polymer electrolytes: In-situ correlation of mechanical, ionic transport, and optical properties, J. Electrochem. Soc. 161 (6) (2014) E112–E117.
[9] T. Kelly, B. Ghadi, S. Berg, H. Ardebili, In situ study of strain-dependent ion conductivity of stretchable polyethylene oxide electrolyte, Sci. Rep. 6 (2016) 20128.
[10] E.L. Asp, Multifunctional composite materials for energy storage in structural load paths, Plast. Rubber Comp. 42 (4) (2013) 144–149.
[11] D. Grazioli, V. Zadin, D. Brandell, A. Simone, Electrochemical-mechanical modeling of solid polymer electrolytes: Stress development and non-uniform electric current density in trench geometry microbatteries, Electrochim. Acta (2018), https://doi.org/10.1016/j.electacta.2018.07.146.
[12] D. Grazioli, M. Magri, A. Salvadori, Computational modeling of Li-ion batteries, Comput. Mech. 58 (6) (2016) 889–909.
[13] P.P. Natsiavas, K. Weinberg, D. Rosato, M. Ortiz, Effect of prestress on the stability of electrode-electrolyte interfaces during charging in lithium batteries, J. Mech. Phys. Solid. 95 (2016) 92–111.
[14] G. Bucci, Y.-M. Chiang, W. Carter, Formulation of the coupled electrochemical-mechanical boundary-value problem, with applications to transport of

multiple charged species, Acta Mater. 104 (2016) 33–51.
[15] J. Snyder, E. Wetzel, C. Watson, Improving multifunctional behavior in structural electrolytes through copolymerization of structure- and conductivity-promoting monomers, Polymer 50 (20) (2009) 4906–4916.
[16] B. Scrosati, C.A. Vincent, Polymer electrolytes: The key to lithium polymer batteries, MRS Bull. 25 (3) (2000) 28–30.
[17] M. Willgert, S. Leijonmarck, G. Lindbergh, E. Malmstrom, M. Johansson, Cellulose nanofibril reinforced composite electrolytes for lithium ion battery applications, J. Mater. Chem. A 2 (33) (2014) 13556–13564.
[18] M. Moreno, R. Quijada, M.S. Ana, E. Benavente, P. Gomez-Romero, G. González, Electrical and mechanical properties of poly(ethylene oxide)/intercalated clay polymer electrolyte, Electrochim. Acta 58 (2011) 112–118.
[19] Q. Feng, J. Yang, Y. Yu, F. Tian, B. Zhang, M. Feng, S. Wang, The ionic conductivity, mechanical performance and morphology of two-phase structural electrolytes based on polyethylene glycol, epoxy resin and nano-silica, Mater. Sci. Eng. B 219 (2017) 37–44.
[20] X. Su, T. Zhang, X. Liang, H. Gao, B. Sheldon, Employing nanoscale surface morphologies to improve interfacial adhesion between solid electrolytes and Li ion battery cathodes, Acta Mater. 98 (2015) 175–181.
[21] J. Long, B. Dunn, D. Rolison, H. White, Three-dimensional battery architectures, Chem. Rev. 104 (10) (2004) 4463–4492.
[22] D. Danilov, R.A.H. Niessen, P.H.L. Notten, Modeling all-solid-state Li-ion batteries, J. Electrochem. Soc. 158 (3) (2011) A215–A222.
[23] D. Danilov, P.H.L. Notten, Mathematical modelling of ionic transport in the electrolyte of Li-ion batteries, Electrochim. Acta 53 (17) (2008) 5569–5578.
[24] A. Salvadori, D. Grazioli, M. Geers, D. Danilov, P. Notten, A multiscale-compatible approach in modeling ionic transport in the electrolyte of (lithium ion) batteries, J. Power Sources 293 (2015) 892–911.
[25] A. Salvadori, D. Grazioli, M. Magri, M. Geers, D. Danilov, P. Notten, On the role of saturation in modeling ionic transport in the electrolyte of (lithium ion) batteries, J. Power Sources 294 (2015) 696–710.
[26] W. Dreyer, C. Guhlke, R. Muller, Overcoming the shortcomings of the Nernst-Planck model, Phys. Chem. Chem. Phys. 15 (2013) 7075–7086.
[27] S. Braun, C. Yada, A. Latz, Thermodynamically consistent model for space-charge-layer formation in a solid electrolyte, J. Phys. Chem. C 119 (39) (2015) 22281–22288.
[28] A. Bard, L. Faulkner, Electrochemical Methods: Fundamentals and Applications, second ed., Wiley, 2000.
[29] D. Griffith, Introduction to Electrodynamics, first ed., Prentice Hall, 1999.
[30] J. Newman, K. Thomas-Alyea, Electrochemical Systems, third ed., John Wiley and Sons, 2004.
[31] A. Salvadori, D. Grazioli, M. Geers, Governing equations for a two-scale analysis of Li-ion battery cells, Int. J. Solids Struct. 59 (2015) 90–109.
[32] V. Zadin, D. Brandell, Modelling polymer electrolytes for 3D-microbatteries using finite element analysis, Electrochim. Acta 57 (2011) 237–243.
[33] V. Zadin, D. Brandell, H. Kasemägi, A. Aabloo, J. Thomas, Finite element modelling of ion transport in the electrolyte of a 3D-microbattery, Solid State Ionics 192 (1) (2011) 279–283.
[34] V. Zadin, H. Kasemägi, A. Aabloo, D. Brandell, Modelling electrode material utilization in the trench model 3D-microbattery by finite element analysis, J. Power Sources 195 (18) (2010) 6218–6224.
[35] A. Salvadori, E. Bosco, D. Grazioli, A computational homogenization approach for Li-ion battery cells: Part 1–formulation, J. Mech. Phys. Solid. 65 (2014) 114–137.
[36] P. Georén, G. Lindbergh, Characterisation and modelling of the transport properties in lithium battery polymer electrolytes, Electrochim. Acta 47 (4) (2001) 577–587.
[37] M. Landstorfer, S. Funken, T. Jacob, An advanced model framework for solid electrolyte intercalation batteries, Phys. Chem. Chem. Phys. 13 (2011) 12817–12825.
[38] X. Zhang, S. Wei, M.A. Sastry, Numerical simulation of intercalation-induced stress in Li-ion battery electrode particles, J. Electrochem. Soc. 154 (10) (2007) A910–A916.
[39] R. Purkayastha, R. McMeeking, A linearized model for lithium ion batteries and maps for their performance and failure, J. Appl. Mech. 79 (2012) 1–16.
[40] M. Klett, M. Giesecke, A. Nyman, F. Hallberg, R. Lindström, G. Lindbergh, I. Furó, Quantifying mass transport during polarization in a Li ion battery electrolyte by in situ ^{7}Li NMR imaging, J. Am. Chem. Soc. 134 (36) (2012) 14654–14657.
[41] G. Bucci, T. Swamy, Y.-M. Chiang, W. Carter, Modeling of internal mechanical failure of all-solid-state batteries during electrochemical cycling, and implications for battery design, J. Mater. Chem. A 5 (2017) 19422–19430.
[42] A. Amirsadeghi, J. Lee, S. Park, A simulation study on the effect of cross-linking agent concentration for defect tolerant demolding in UV nanoimprint lithography, Langmuir 28 (31) (2012) 11546–11554.
[43] Y. Gan, J. Yin, X. Jiang, Self-wrinkling induced by the photopolymerization and self-assembly of fluorinated polymer at air/liquid interface, J. Mater. Chem. A 2 (43) (2014) 18574–18582.
[44] O. Verners, B. Thijsse, A. van Duin, A. Simone, Salt concentration effects on mechanical properties of $LiPF_6$/poly(propylene glycol) diacrylate solid electrolyte: Insights from reactive molecular dynamics simulations, Electrochim. Acta 221 (2016) 115–123.
[45] J. Snyder, R. Carter, E. Wetzel, Electrochemical and mechanical behavior in mechanically robust solid polymer electrolytes for use in multifunctional structural batteries, Chem. Mater. 19 (2007) 3793–3801.
[46] P. Atkins, J. DePaula, Physical Chemistry, ninth ed., W. H. Freeman and Company, 2010.
[47] Y. Marcus, G. Hefter, Standard partial molar volumes of electrolytes and ions in nonaqueous solvents, Chem. Rev. 104 (7) (2004) 3405–3452.
[48] A. Nyman, M. Behm, G. Lindbergh, Electrochemical characterisation and modelling of the mass transport phenomena in $LiPF_6$-EC-EMC electrolyte, Electrochim. Acta 53 (22) (2008) 6356–6365.
[49] R. Naejus, R. Coudert, P. Willmann, D. Lemordant, Ion solvation in carbonate-based lithium battery electrolyte solutions, Electrochim. Acta 43 (3) (1998) 275–284.
[50] Y. Ma, M. Doyle, T. Fuller, M. Doeff, L. De Jonghe, J. Newman, The measurement of a complete set of transport properties for a concentrated solid polymer electrolyte solution, J. Electrochem. Soc. 142 (6) (1995) 1859–1868.
[51] A. Salvadori, R. McMeeking, D. Grazioli, M. Magri, A coupled model of transport-reaction-mechanics with trapping. Part I–Small strain analysis, J. Mech. Phys. Solid. 114 (2018) 1–30.
[52] M. Ue, Mobility and ionic association of lithium and quaternary ammonium salts in propylene carbonate and γ-butyrolactone, J. Electrochem. Soc. 141 (12) (1994) 3336–3342.
[53] M. Qu, W. Woodford, J. Maloney, W. Carter, Y.-M. Chiang, K. Van Vliet, Nanomechanical quantification of elastic, plastic, and fracture properties of $LiCoO_2$, Adv. Energy Mater. 2 (8) (2012) 940–944.
[54] Y. Qi, L. Hector, C. James, K. Kim, Lithium concentration dependent elastic properties of battery electrode materials from first principles calculations, J. Electrochem. Soc. 161 (11) (2014) F3010–F3018.
[55] L. Wu, W. Lee, J. Zhang, First principles study on the electrochemical, thermal and mechanical properties of $LiCoO_2$ for thin film rechargeable battery, Mater. Today Proc. 1 (1) (2014) 82–93.
[56] J.R. Cost, K.R. Janowski, R.C. Rossi, Elastic properties of isotropic graphite, Philos. Mag. J. Theor. Exp. Appl. Phys. 17 (148) (1968) 851–854.
[57] Y. Qi, H. Guo, L. Hector Jr., A. Timmons, Threefold increase in the Young's modulus of graphite negative electrode during lithium intercalation, J. Electrochem. Soc. 157 (5) (2010) A558–A566.
[58] F. Yang, Interaction between diffusion and chemical stresses, Mater. Sci. Eng. A 409 (2005) 153–159.
[59] A. Talin, D. Ruzmetov, A. Kolmakov, K. McKelvey, N. Ware, F. El Gabaly, B. Dunn, H. White, Fabrication, testing, and simulation of all-solid-state three-dimensional Li-ion batteries, ACS Appl. Mater. Interfaces 8 (47) (2016) 32385–32391.
[60] W. Woodford, Y.-M. Chiang, W. Carter, "Electrochemical shock" of intercalation electrodes: A fracture mechanics analysis, J. Electrochem. Soc. 157 (10) (2010) A1052–A1059.
[61] Wolfram Research, Inc, Mathematica, Version 10, 4 Edition, Wolfram Research, Inc., 2016. URL, https://www.wolfram.com/mathematica/.
[62] G. Bucci, T. Swamy, Y.-M. Chiang, W. Carter, Random walk analysis of the effect of mechanical degradation on all-solid-state battery power, J. Electrochem. Soc. 164 (12) (2017) A2660–A2664.
[63] V. Zadin, D. Brandell, H. Kasemägi, J. Lellep, A. Aabloo, Designing the 3D-microbattery geometry using the level-set method, J. Power Sources 244 (2013) 417–428.
[64] A. Panteghini, L. Bardella, On the finite element implementation of higher-order gradient plasticity, with focus on theories based on plastic distortion incompatibility, Comput. Methods Appl. Mech. Eng. 310 (2016) 840–865.
[65] A. Mukhopadhyay, B. Sheldon, Deformation and stress in electrode materials for Li-ion batteries, Prog. Mater. Sci. 63 (2014) 58–116.
[66] Y. Wang, B. Liu, Q. Li, S. Cartmell, S. Ferrara, Z. Deng, J. Xiao, Lithium and lithium ion batteries for applications in microelectronic devices: A review, J. Power Sources 286 (2015) 330–345.
[67] M. Kumar, S. Sekhon, Role of plasticizer's dielectric constant on conductivity modification of PEO–NH_4F polymer electrolytes, Eur. Polym. J. 38 (7) (2002) 1297–1304.
[68] S. Ketabi, K. Lian, Effect of SiO_2 on conductivity and structural properties of PEO–$EMIHSO_4$ polymer electrolyte and enabled solid electrochemical capacitors, Electrochim. Acta 103 (2013) 174–178.
[69] S. Goswami, A. Dutta, Conductivity studies of plasticized proton conducting PVA–PVIM blend doped with NH_4BF_4, Ionics 19 (8) (2013) 1125–1134.
[70] X.-L. Wu, S. Xin, H.-H. Seo, J. Kim, Y.-G. Guo, J.-S. Lee, Enhanced Li^+ conductivity in PEO–LiBOB polymer electrolytes by using succinonitrile as a plasticizer, Solid State Ionics 186 (1) (2011) 1–6.
[71] D. Pradhan, R. Choudhary, B. Samantaray, Studies of dielectric and electrical properties of plasticized polymer nanocomposite electrolytes, Mater. Chem. Phys. 115 (2) (2009) 557–561.
[72] S. Plimpton, Fast parallel algorithms for short-range molecular dynamics, J. Comput. Phys. 117 (1) (1995) 1–19.
[73] A. van Duin, S. Dasgupta, F. Lorant, W. Goddard, ReaxFF: A reactive force field for hydrocarbons, J. Phys. Chem. A 105 (41) (2001) 9396–9409.
[74] A. Rappe, W. Goddard, Charge equilibration for molecular dynamics simulations, J. Phys. Chem. 95 (8) (1991) 3358–3363.
[75] H.M. Aktulga, J.C. Fogarty, S.A. Pandit, A.Y. Grama, Parallel reactive molecular dynamics: Numerical methods and algorithmic techniques, Parallel Comput. 38 (4) (2012) 245–259.
[76] M. Islam, V. Bryantsev, A. van Duin, ReaxFF reactive force field simulations on the influence of teflon on electrolyte decomposition during Li/SWCNT anode

discharge in lithium-sulfur batteries, J. Electrochem. Soc. 161 (8) (2014) E3009–E3014.
[77] M. Ong, O. Verners, E. Draeger, A. van Duin, V. Lordi, J. Pask, Lithium ion solvation and diffusion in bulk organic electrolytes from first-principles and classical reactive molecular dynamics, J. Phys. Chem. B 119 (4) (2015) 1535–1545.
[78] C. Svaneborg, G.S. Grest, R. Everaers, Disorder effects on the strain response of model polymer networks, Polymer 46 (12) (2005) 4283–4295.